Available online at www.sciencedirect.com

ScienceDirect

Geochimica et Cosmochimica Acta 216 (2017) 335–357

Geochimica et Cosmochimica Acta

www.elsevier.com/locate/gca

Homogenisation of sulphide inclusions within diamonds: A new approach to diamond inclusion geochemistry

Iain McDonald [a,*], Hannah S.R. Hughes [b,1], Ian B. Butler [c], Jeffrey W. Harris [d], Duncan Muir [a]

[a] School of Earth and Ocean Sciences, Cardiff University, Park Place, Cardiff CF10 3AT, UK
[b] School of Geosciences, University of the Witwatersrand, Private Bag 3, Wits 2050, Johannesburg, South Africa
[c] School of Geosciences, University of Edinburgh, Edinburgh EH9 3JW, UK
[d] School of Geographical and Earth Sciences, University of Glasgow, Glasgow G12 8QQ, UK

Received 11 November 2016; accepted in revised form 28 April 2017; available online 8 May 2017

Abstract

Base metal sulphide (BMS) inclusions in diamonds provide a unique insight into the chalcophile and highly siderophile element composition of the mantle. Entombed within their diamond hosts, these provide a more robust (closed system) sample, from which to determine the trace element, Re-Os and S-isotopic compositions of the mantle than mantle xenoliths or orogenic peridotites, as they are shielded from alteration during ascent to the Earth's crust and subsequent surface weathering. However, at temperatures below 1100 °C some BMS inclusions undergo subsolidus re-equilibration from an original monosulphide solid solution (Mss) and this causes fractionation of the major and trace elements within the inclusions. Thus to study the subjects noted above, current techniques require the *entire* BMS inclusion to be extracted for analyses. Unfortunately, 'flaking' of inclusions during break-out is a frequent occurrence and hence the risk of accidentally under-sampling a portion of the BMS inclusion is inherent in current practices. This loss may have significant implications for Re-Os isotope analyses where incomplete sampling of a Re-rich phase, such as chalcopyrite that typically occurs at the outer margins of BMS inclusions, may induce significant bias in the Re-Os and $^{187}Os/^{188}Os$ measurements and resulting model and isochron ages.

We have developed a method for the homogenisation of BMS inclusions in diamond prior to their break-out from the host stone. Diamonds are heated to 1100 °C and then quenched to chemically homogenise any sulphide inclusions for both major and trace elements. Using X-ray Computed Microtomography (μCT) we determine the shape and spatial setting of multiple inclusions within a host stone and crucially show that the volume of a BMS inclusion is the same both before and after homogenisation. We show that the homogenisation process significantly reduces the inherent variability of *in situ* analysis when compared with unhomogenised BMS, thereby widening the scope for multiple methods for quantitative analysis, even on 'flakes' of single BMS inclusions. Finally we show that the trace elements present in peridotite (P-type) and eclogitic (E-type) BMS are distinct, with P-type diamonds having systematically higher total platinum-group element (particularly

Abbreviations: PGE, platinum-group elements; IPGE, Ir-group PGE; PPGE, Pd-group PGE; Mss, monosulphide solid solution; Iss, intermediate solid solution

* Corresponding author.
E-mail address: McDonaldi1@cf.ac.uk (I. McDonald).
[1] Present address: Camborne School of Mines, College of Engineering, Mathematics and Physical Sciences, University of Exeter, Penryn Campus, Penryn TR10 9FE, UK.

http://dx.doi.org/10.1016/j.gca.2017.04.039
0016-7037/

Os, Ir, Ru) and Te and As concentrations. These distinctions suggest that the PGE and semi-metal budgets of mantle-derived partial melts will be significantly dependent upon the *type(s)* and proportions of sulphides present in the mantle source.

Keywords: Diamond; Sulphide inclusion; Homogenisation; PGE; Re-Os isotopes; Semi-metals

1. INTRODUCTION

Inclusions encapsulated within diamonds provide a rare opportunity to sample deep-seated mantle silicates, sulphides, fluids, metals or metal alloys. Diamonds are generally considered to be robust containers for these inclusions, effectively shielding them chemically during their ascent to the Earth's surface and preserving their composition. Inclusions are generally thought to have been formed syngenetically with the host diamond (as indicated by the imposed diamond morphology of the inclusions e.g., Sobolev, 1977; Meyer, 1987; Bulanova, 1995; Richardson et al., 2001, 2004 – although see Taylor and Anand, 2004; Agrosì et al., 2016; Nestola et al., 2017 for a different viewpoint) and their study thus allows us an insight into mantle geochemistry, geodynamics, and diamond mineralisation processes that cannot be achieved by other means.

Base metal sulphides (BMS) are among the most common types of inclusion found in diamonds (e.g., Harris and Gurney, 1979; Stachel and Harris, 2008). BMS occur in both major diamond parageneses, being relatively Ni-rich in peridotitic (P-type) diamond and relatively Ni-poor when associated with eclogitic (E-type) diamonds. Their relative abundance may itself be informative for understanding diamond mineralisation where transient volatile-rich (C, H, O, N, S) metasomatic agents have been suggested as key to diamond formation (e.g., Deines and Harris, 1995; Westerlund et al., 2004; Thomassot et al., 2007, 2009; Stachel and Luth, 2015). Thus studies of BMS inclusions within diamonds have become a major line of enquiry; for the timing and genesis of diamond growth, for models of crustal and mantle development during the Archaean and the Earth's deep carbon cycle (e.g., Hart et al., 1997; Pearson et al., 1998; Richardson et al., 2001, 2009; Shirey et al., 2004; Stachel and Harris, 2008; Dasgupta and Hirschmann, 2010; Harvey et al., 2016).

The first attempts to measure the trace element chemistry of whole diamonds containing BMS inclusions were made by Fesq et al. (1973, 1975) using instrumental neutron activation analysis (INAA). They detected 40 trace elements, including the highly siderophile elements Au and Ir. With these early studies, however, instrumental limitations and lack of suitable standard materials meant that it was only in the 1990s that quantified concentrations of trace elements in inclusion-bearing whole diamonds were first published (Schrauder et al., 1996; Damarupurshad et al., 1997; Hart et al., 1997). In particular, Hart et al. (1997) noted a distinction between the Au/Ir ratios of P-type diamonds (Au/Ir < 0.3) and E-type diamonds (Au/Ir ranging 0.3–100) and they linked this difference to protoliths involving melt-depleted cratonic mantle and subducted former oceanic lithosphere, respectively.

The INAA studies cited above involved analysis of whole diamonds, generally containing BMS and other inclusions, rather than BMS inclusions alone. The first attempt to analyse a suite of chalcophile trace elements in extracted BMS inclusions was made by McDonald et al. (1996) who dissolved extracted BMS and used inductively coupled plasma-mass spectrometry (ICP-MS). These authors determined the platinum-group elements (PGE), alongside Re and Au and the major elements (Fe, Ni, Cu), in two single inclusions and one composite sample (comprising multiple inclusions from the same stone), extracted from three E-type diamonds from the Orapa mine in Botswana. Ruthenium, Rh, Pd and Au were measurable at ppm to 10's of ppm concentrations both in single inclusions and the composite sample but Ir, Pt and Re were below detection. Osmium was not analysed due to the volatilsation and loss of OsO_4 during the dissolution stage. In the same year Bulanova et al. (1996) analysed PGE and semi-metals at 10's–100's of ppm concentrations in BMS inclusions in Yakutian P-type and E-type diamonds by micro-PIXE (particle-induced X-ray emission) and found a strong enrichment in the Ir-group PGE (IPGE – Os, Ir and Ru) over the palladium-group PGE (PPGE – Rh, Pt and Pd).

Advances in laser ablation ICP-MS (LA-ICP-MS) and in the development of sulphide standards for *in situ* analysis of PGE and Au in BMS have led to rapid advances in the study of mantle sulphides (see recent reviews by Luguet and Reisberg, 2016; Harvey et al., 2016). But aside from work primarily devoted towards Re-Os isotopes there have been comparatively few studies dedicated to analysing trace elements in diamond-hosted BMS since the 1990s. The work by Aulbach et al. (2012) on BMS in E-type diamonds from the Slave craton is the only recent study to provide comprehensive PGE, Au, Re and semi-metal data for diamond-hosted BMS inclusions.

This paucity of results may arise from the fact that the sulphides themselves present a number of problems for geochemical and isotopic investigations, stemming from the re-equilibration of high temperature monosulphide solid solution (Mss) to Fe-, Ni- and Cu-rich endmembers during cooling (Naldrett, 1989, 2011; Taylor and Liu, 2009). This process is summarised in Fig. 1. The PGE, Au, Re and semi-metals partition and fractionate between the different Fe-, Ni- and Cu-rich sulphide minerals and may also form discrete platinum-group minerals (PGM) or gold-rich minerals such as tellurides (e.g. Fleet et al., 1993; Barnes et al., 1997; Mungall et al., 2005; Helmy et al., 2007; Taylor and Liu, 2009; Holwell and McDonald, 2010). Because of this fractionation, it is incumbent that all of the mass of the inclusion be extracted intact to ensure a completely unbiased estimate for the composition of the original bulk

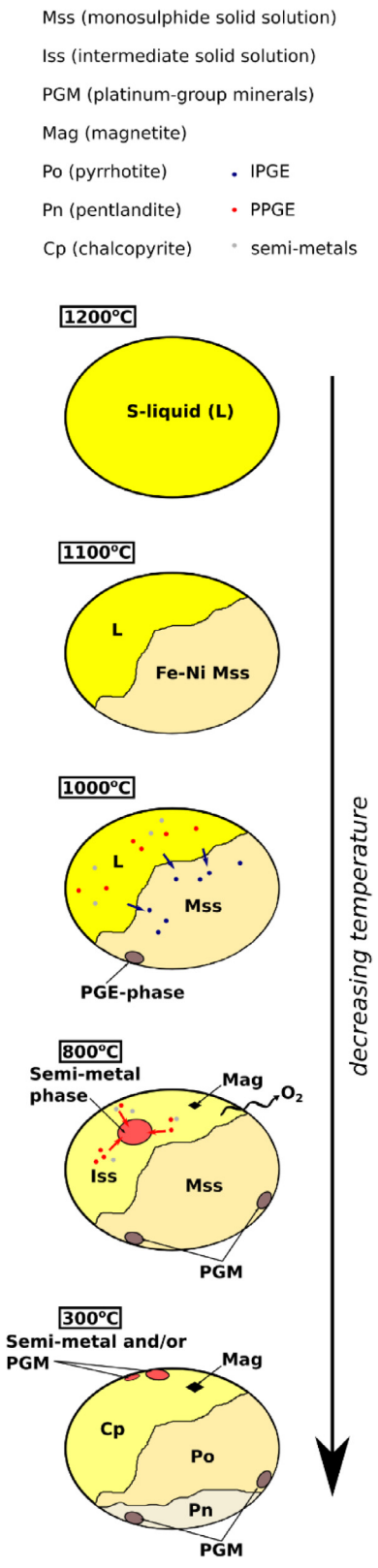

Fig. 1. Schematic timeline for the cooling and crystallisation of a sulphide liquid to monosulphide solid solution (Mss), intermediate solid solution (ISS), a semimetal immiscible phase and low-temperature mineral phases. Adapted from Holwell and McDonald (2010).

sulphide (Richardson et al., 2001; Taylor and Liu, 2009; Harvey et al., 2016). However, the 'flaking' or disintegration of the sulphide during inclusion extraction by breaking open the diamond, is a frequently documented and inherent problem (e.g., Deines and Harris, 1995; Pearson et al., 1998; Richardson et al., 2001, 2009; Thomassot et al., 2009). Thus, partial sampling of BMS inclusions is common and may introduce a serious bias to geochemical and/or isotopic results and classifications. The partitioning studies cited above demonstrate that a fragment of the Cu-rich endmember of the fractionated inclusion will have significantly higher Re, Au, Pt and Pd and lower Ni, Ir, Os and Ru abundances than the Ni-rich counterpart from the same inclusion (and vice versa). This is compounded by the fact that Cu-rich sulphides are commonly observed to have exsolved to the edges of BMS inclusions and are therefore most susceptible to flaking and incomplete sampling when the diamond is broken.

The genesis ages of BMS inclusions in diamond have been determined as either model ages, or more commonly, as isochrons using Re-Os isotopic systematics (e.g., Pearson et al., 1998; Richardson et al., 2001; Carlson, 2005; Stachel and Harris, 2008; Harvey et al., 2016 and references therein). These results are also reliant upon measuring the *total* sulphide composition. Due to the intrinsically different compatibility of Re (into the Cu-rich endmember) from Os (into the Ni-Fe endmember) in the re-equilibrating sulphide (Fig. 2) these elements may become significantly fractionated from one another. Further complications arise if Re partitions into any PGM (e.g., Wainwright et al., 2016). Fractionation may start at any time *after* the sulphide has been encapsulated in the diamond and the isotopic implications are dependent upon the timing and length of the fractionation. For example, the similar Os-isotopic composition ($^{187}Os/^{188}Os$ or expressed as γ_{Os}) of the core (Ni-(Os)-rich) vs rim (Cu-(Re)-rich) of a differentiated sulphide inclusion from a single Kimberley diamond was used by Richardson et al. (2001) to suggest that fractionation of the sulphide took place during, or just prior to, transport of the diamond to the surface in the Cretaceous (Richardson et al., 2001). Whilst in this case fractionation apparently had little effect on the Re-Os isotopic systematics of the inclusion, this may not be the case for inclusions that have been held at temperatures beneath the Mss liquidus for long periods of time, or especially for diamonds from geologically old kimberlites where BMS inclusions have fully fractionated and potential for in-growth of ^{187}Os into chalcopyrite is maximised. This potential sampling problem is inherent in all approaches that rely on unhomogenised sulphide inclusions regardless of whether fragments are analysed by wet chemistry or *in situ* by LA-ICP-MS, electron microscopy or ion beam techniques.

Sulphur isotopic compositions (particularly $\delta^{34}S$) may also be affected by partial sampling of inclusions, as instrumental mass-fractionation is sensitive to the endmember sulphide analysed (e.g., Chaussidon et al., 1987; Thomassot et al., 2009). Sulphide inclusions in Orapa diamonds show a range in $\delta^{34}S$ from +2.1 to +9.5‰ (pyrrhotite, Chaussidon et al., 1987) to −11 to +2‰ (Mss and pyrrhotite, Eldridge et al., 1991). More recently, a smaller

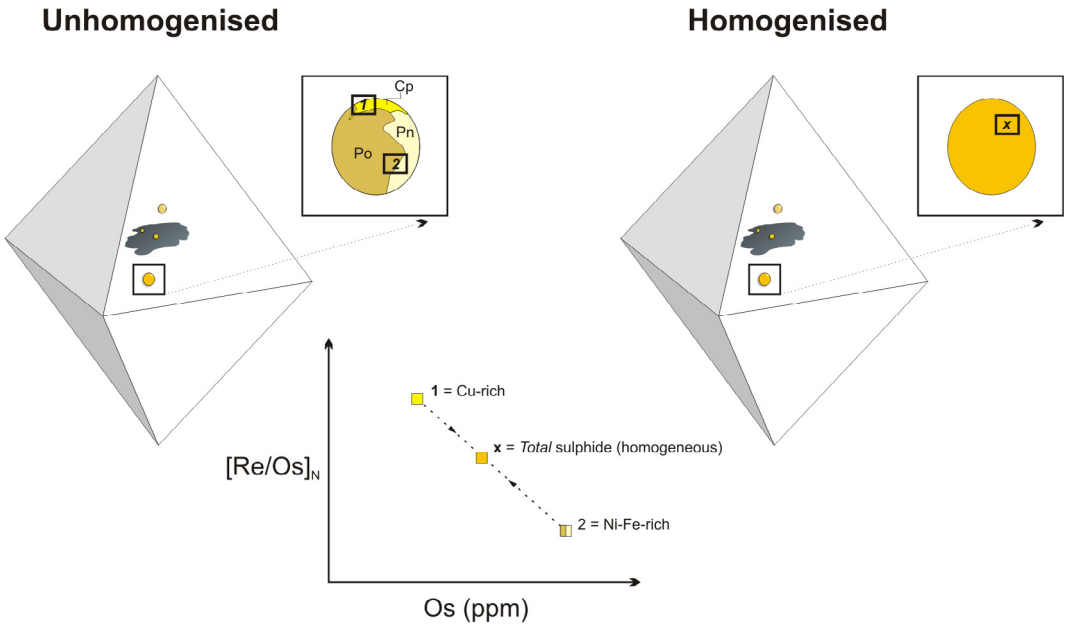

Fig. 2. Schematic diagram demonstrating the problems regarding partial sampling of a fractionated (unhomogenised) sulphide inclusion and its apparent geochemistry vs partial sampling of a homogenised and quenched sulphide inclusion.

range of pyrrhotite inclusion $\delta^{34}S$ compositions, from −1.4 to +2.6‰, has been reported by Farquhar et al. (2002). We note that the study by Farquhar et al. (2002) used inclusions with a smaller range in Ni-content, either suggesting that a subset of the Orapa sulphide population was represented in their 2002 study and/or that preceding studies could exemplify a degree of bias in sampling fragmented inclusions. Mass-independent fraction $\Delta^{33}S$ in the Farquhar et al. (2002) study reported a range from −0.1 to + 0.6‰. In all cases, the range of $\delta^{34}S$ and $\Delta^{33}S$ has been used to infer an isotopic signature for both younger (<2.45 Ga) and older (>2.45 Ga) subduction of S-bearing sediments, as recorded in the mantle (e.g., Farquhar et al., 2002; Thomassot et al., 2009).

In principle if the diamond remains a closed system then BMS inclusions could be homogenised (through a process of re-melting and rapid quenching) as part of the sample preparation *prior* to sulphide inclusion break-out from the diamond host. This would eliminate any partial sampling bias and effectively mean that any fragment of a homogenised inclusion is representative (geochemically and isotopically) of the total sulphide composition encased within the diamond originally. Such a process would potentially provide a new and rigorous test of sulphide inclusion geochemical variability across diamond suites or in cases where there are multiple inclusions within a single diamond host crystal. In particular, it would deliver a more robust sampling system for Re-Os isotopic analyses where accidental sampling bias (leading to the exclusion of Re and potentially ^{187}Os-rich chalcopyrite) may have detrimental effects on calculations of model ages and initial ratios (e.g. Richardson et al., 2001; Shirey et al., 2013; Harvey et al., 2016). The homogenisation method we describe below permits analysis of sulphide inclusions for both major elements by fully quantitative scanning electron microscopy (SEM) and energy dispersive spectrometry (EDS) and trace elements (by LA-ICP-MS) which allows use of the same inclusions for a full geochemical suite of elements, avoids any volatilisation problem of Os, and allows for direct calculation of S/metal and S/Se ratios pertinent to identifying if metal alloy phases are present within the sulphide (e.g., Fleet et al., 1991).

2. DIAMOND SAMPLES

The diamonds and BMS inclusions used in this study are from the Orapa kimberlite in NE Botswana, the mine being situated on the western edge of the Kaapvaal-Zimbabwe Craton (Kalahari Craton) within the 2.1–1.9 Ga Magondi orogenic belt (Fig. 3; Silver et al., 2004 and references therein). The pipe has a Cretaceous eruption age of c. 93 Ma (Davis, 1977; Haggerty et al., 1983). The genesis age of Orapa diamonds was first estimated to be 990 ± 50 Ma (based on a Nd/Sm isochron; Richardson, 1989) but more recently Ar-Ar dating of clinopyroxene inclusions have given genesis ages of 906–1032 Ma with a minor group of older diamonds at >2500 Ma (Burgess et al., 2004). Sulphide inclusions from Orapa E-type diamonds have been dated (Re-Os model age) to include multiple ages of between 2.5–3.0 Ga and 1.0 Ga (see Shirey et al., 2001, 2002 and references therein).

The sub-solidus sulphide mineralogy from Orapa inclusions in diamond has been previously reported by Deines and Harris (1995). From random polished sections, almost half of the 21 inclusions studied by these authors comprised only pyrrhotite (10). The remaining inclusions comprised monosulphide solid solution (4), a mixture of pyrrhotite and pentlandite (4), pyrrhotite-pentlandite-chal

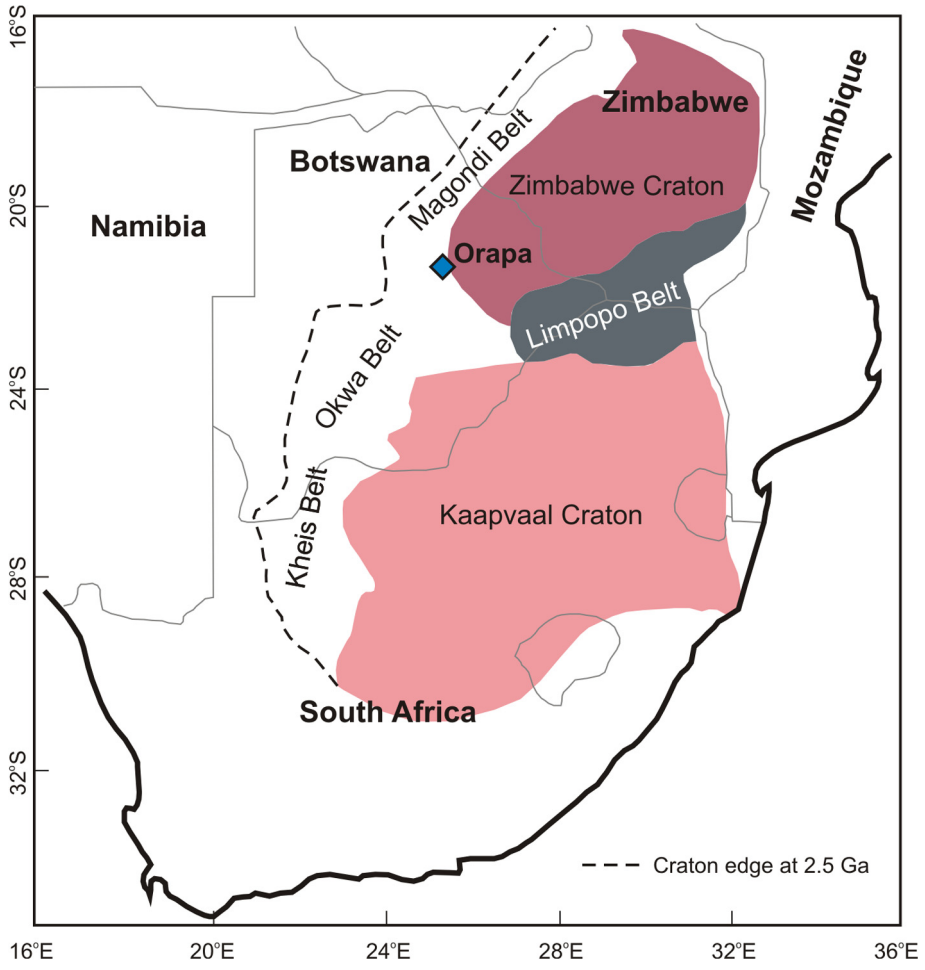

Fig. 3. Location map of Orapa, Magondi Belt and the Kaapvaal-Zimbabwe Craton. Adapted from Shirey et al. (2001), McCourt et al. (2004) and Shirey et al. (2004).

copyrite (2) and pentlandite-chalcopyrite (1). Based on the Ni-content of the sulphides, approximately 85% of these inclusions from Orapa are thought to be from the eclogite paragenesis (on the basis of <8% Ni; Yefimova et al., 1983).

Five colourless diamonds (see Table 1), each approximately 4 mm in diameter and of 1 carat weight were used for experiments in this study. In all cases there were no fractures to the surface of the stones from the inclusions. Diamond H1 was a dodecahedral macle and its rounded surface prevented clear internal viewing, but a prominent black metallic rosette fracture within the central portion of the diamond was still visible. Diamond H2 was an elongate octahedron with negative trigons on many of the octahedral surfaces. At least four metallic rosette fractures were visible within this specimen, and the sulphide 'eyes' within these systems could be seen. Diamond H3 was a colourless well-shaped octahedron with slightly rounded edges and exhibiting negative trigons on most faces. Apart from a relatively large single sulphide rosette in the centre of the stone some smaller sulphides were noted in later analysis (see Section 5.3). Inclusion sizes ranged from about 50 to 200 μm. Diamond IM2 was a colourless broken dodecahedron and IM6 was a colourless elongate rounded octahedron. Based on external morphology, the diamonds showed no evidence of plastic deformation.

3. EXPERIMENTAL METHODS

The main aim of our experimental process is to heat all sulphide inclusion(s) within the diamond host to a temperature above the Mss liquidus (1100 °C – see for example Kullerud and Yoder, 1959; Arnold, 1971; Bowles et al., 2011) allowing all sulphide phases to fully homogenise, and thereafter to quench the inclusion so rapidly that sulphide fractionation is minimised to the extent that the scale of any remaining heterogeneity is at a grain size below the scale of sampling used by SEM or LA-ICP-MS. Thus the major and trace element composition of the sulphide inclusions are made uniform and any partial sample extracted from the diamond will be representative of the average composition of the inclusion (Fig. 2). This process is similar to that used for preparation of homogenised sulphide inclusions in chromitites by Holwell et al. (2011).

Table 1
List of homogenised and unhomogenised diamond samples and their sulphide inclusions, including dimensions of inclusions and fragments.

Details of sulphide inclusions				
Diamond	Sample	Dimensions (μm)	Details of fragment/inclusion	Homogenised/Unhomogenised
H1	H1a	150 × 100 × 100	Fragment from mixed multiple inclusions	Homogenised
	H1b	100 × 100 × 80	Fragment from mixed multiple inclusions	Homogenised
	H1c	100 × 100 × 80	Fragment from mixed multiple inclusions	Homogenised
	H1d	150 × 100 × 30	Fragment from mixed multiple inclusions	Homogenised
	H1e	200 × 100 × 30	Fragment from mixed multiple inclusions	Homogenised
H2	H2a	200 × 150 × 150	Whole inclusion – #1 of 4	Homogenised
	H2b	150 × 100 × 100	Whole inclusion – #2 of 4	Homogenised
H3	H3a	100 × 50 × 50	Fragment of inclusion – #1 of 5	Homogenised
IM2	IM2a	300 × 150 × 100	Fragment of single inclusion	Unhomogenised
	IM2b	350 × 300 × 250	Fragment of single inclusion	Unhomogenised
IM6	IM6a	300 × 200 × 150[a]	Fragment of single inclusion	Unhomogenised

[a] Original size of whole inclusion which subsequently broke (sample IM6a is a fragment of this original).

The homogenisation experiments were performed at the University of Edinburgh's (UK) Experimental Geoscience Facility. A vertical tube 1 atmosphere furnace was connected to H_2 and CO_2 gas supplies via Bronkhorst™ gas mass flow controllers to establish a defined fO_2 at the furnace hotspot. The hotspot temperature used was 1100 °C, and a gas mix of 14% H_2 and 86% CO_2 was used to ensure a calculated fO_2 environment between $10^{-11.3}$ and $10^{-11.4}$ (i.e., QFM-1 buffer; Deines, 1974) to prevent the diamond from combusting and the sulphide inclusion from oxidising. Due to space restrictions within the tube furnace and the strict location of the 'hot spot' at the target temperature within it, each of the three diamonds to be homogenised were run separately through the experimental set-up. The diamond was suspended in a cradle of machinable alumina and Pt wire and positioned within the cold portion at the top of the tube furnace whilst the furnace was flushed with CO_2 gas. After flushing with CO_2, the CO_2/H_2 mix was allowed to stabilise for 5 min before the sample was lowered to the hot spot of the furnace. Based on the relative size of the diamonds compared with the 1 cm^3 chromitite blocks successfully homogenised by Holwell et al. (2011) each specimen was allowed to homogenise for 15 min. For rapid quenching, the Pt-wire hanger of the crucible was electrically fused, releasing the diamond (and cradle) to drop out of the furnace and into a cold water trap attached to the base of the tube furnace. Before recovery, the furnace was flushed with pure CO_2 for 10 min to remove H_2 from the furnace before the quench trap was removed.

The very different relative thermal expansion of diamond and the sulphide inclusion typically results in a rosette fracture system being observed around BMS inclusions in diamond (Taylor and Liu, 2009). Whilst these fracture systems may further develop during heating, in the present cases, none were sufficient to break the diamonds used in the experiments, thus the geochemical systems of the sulphide inclusions were not compromised.

After homogenisation and quenching, the faces of the diamonds showed nothing more than a mild 'frosting' effect and no internal fractures were observed to penetrate the outer surfaces, which remained intact. On diamond H1, these etch marks were distributed unevenly across the crystallographic faces, principally because the diamond was a rounded dodecahedron, But for diamond H2, an octahedron, the etching patterned showed negative trigons on octahedral faces. In both cases, no surface graphite was noted. The surface etching is likely the result of the CO_2/H_2 gas mix flowing through the furnace.

4. ANALYTICAL TECHNIQUES

4.1. X-ray Computed Microtomography (μCT)

Tomographic data from diamond H3 (Table 1) was acquired before and after homogenisation using the μCT instrument designed and built at the University of Edinburgh. The instrument comprised a 10–160 kV Feinfocus transmission X-ray source, a MICOS UPR-160-Air rotary table and a Perkin Elmer XRD0822 1 megapixel flat panel amorphous silicon detector with a Gd2O2S:Tb scintillator, operated by control software developed in-house. For the whole diamond scan we used 600 projections and the voxel size of the reconstructed data was 6.2 μm. For the inclusion scan we used 2000 projections and the voxel size was 2.0 μm. All scans were carried out at 100 kV peak energy using a 2 s exposure for each projection collected through a 360° sample rotation. The target power was 2.7 W. Tomographic slices were reconstructed by filtered back projection using Octopus 8.7 (Vlassenbroeck et al., 2007) and visualised in 2D and 3D using Fiji and Avizo 9 software.

4.2. Sulphide inclusion recovery and preparation

Following homogenisation the sulphides were recovered from the diamond by standard break-out methods (Harris and Gurney, 1979; Stachel and Harris, 2008). The inclusions that had undergone experimental homogenisation were not recovered completely whole and broke during recovery. As such, a sub-selection of inclusions (listed in Table 1) were mounted in epoxy resin-filled stubs and

Table 2
Summary table of the major element compositions of homogenised and unhomogenised diamond inclusion samples. Data are from SEM EDS. Refer to supplementary Table C for all point analyses and supplementary Fig. B for a bar chart displaying data from Table 2.

Sample #	Diamond #	Fragment #	Homogenised?	End-member mineral	n	S (wt.%)	Fe	Co	Ni	Cu	Total
H1a	H1	a	Homogenised	n/a (mean)	9	38.97	53.16	0.52	3.28	3.97	99.89
				2σ		0.15	0.63	0.04	0.18	0.34	0.51
H1b	H1	b	Homogenised	n/a (mean)	3	38.88	53.50	0.58	3.32	3.05	99.33
				2σ		0.34	0.18	0.10	0.03	0.33	0.82
H1c	H1	c	Homogenised	n/a (mean)	7	39.00	53.03	0.50	3.21	3.87	99.60
				2σ		0.09	0.37	0.04	0.10	0.32	0.29
H1d	H1	d	Homogenised	n/a (mean)	9	38.82	53.38	0.53	3.33	3.22	99.29
				2σ		0.08	0.19	0.04	0.09	0.20	0.29
H2a	H2	a	Homogenised	n/a (mean)	8	39.46	54.41	0.54	3.01	1.70	99.13
				2σ		0.29	0.33	0.03	0.05	0.06	0.41
H2b	H2	b	Homogenised	n/a (mean)	4	39.50	54.32	0.63	2.97	1.87	99.29
				2σ		0.75	0.21	0.04	0.03	0.20	0.50
H3a	H3	a	Homogenised	n/a (mean)	9	39.08	55.93	0.50	1.40	2.19	99.09
				2σ		0.15	0.30	0.08	0.04	0.10	0.37
IM2a	IM2	a	Unhomogenised	Po (mean)	14	39.41	56.48	0.40	3.35	0.14	99.79
				2σ		0.52	3.15	0.33	3.06	0.06	
				Pn (mean)	4	33.69	27.51	1.01	35.23	1.73	99.17
				2σ		0.50	1.43	0.14	2.40	1.08	
				Cp (mean)	17	35.35	30.99	0.14	1.23	32.62	100.33
				2σ		0.27	0.74	0.17	2.21	2.07	
IM2b	IM2	b	Unhomogenised	Po (mean)	10	40.05	55.86	0.47	4.05	0.14	100.57
				2σ		0.46	3.37	0.41	3.62	0.19	
				Cp (mean)	18	35.77	30.84	0.11	0.66	32.69	100.07
				2σ		0.39	1.26	0.09	1.19	1.14	
IM6a	IM6	a	Unhomogenised	Po (mean)	19	39.39	57.09	0.40	2.04	0.34	99.27
				2σ		0.38	1.44	0.17	1.36	1.62	
				Pn (mean)	5	34.83	33.64	1.22	30.41	0.54	100.63
				2σ		1.29	5.60	0.11	6.45	0.52	
				Cp (mean)	13	35.15	33.35	0.11	0.37	30.49	99.47
				2σ		0.59	3.80	0.10	0.60	4.29	

polished to 0.25 μm grade, using aluminium oxide polishing powder. The largest inclusions (whole or broken fragments) were preferentially chosen in order to test if the homogenisation was successful.

Unhomogenised sulphide inclusions IM2a, IM2b and IM6a that did not undergo this experimental procedure were used for comparison. The details of these inclusions can also be found in Table 1.

4.3. SEM imaging, element mapping and quantitative analysis

Backscattered electron (BSE) images were obtained for each inclusion studied using a Zeiss Sigma HD Scanning Electron Microscope at Cardiff University at operating conditions of 20 kV with ~1 nA beam current. Element mapping was performed using dual 150 mm^2 active area EDS detectors fitted to the SEM and Oxford Instruments Aztec software at operating conditions of 20 kV and ~2 nA. Maps were acquired with a step-size between 0.5 and 1 μm and a pixel dwell time of 15–20 ms at a working distance of 8.9 mm. Quantitative spot and area microanalyses were obtained using the same equipment with Co as a reference standard to measure beam drift every 15 min. Elements were calibrated prior to analysis with MicroAnalysis Consultants Ltd and Astimex Standards Ltd metal and mineral standards. Accuracy and precision of SEM chemical data was measured using Astimex chalcopyrite and pentlandite standards (Supplementary Table A). Repeated spot analyses at the beginning and end of the analytical session demonstrate relative accuracies of 0.4–2.6% for S, 0.1–0.8% for Cu, 0.8–2.7% for Ni, 0.3–3.2% for Fe and 23–41% for Co (at a concentration of 0.43 wt.%). 1σ precision on these repeated measurements was ≤0.23 wt.% for S, ≤0.30 wt.% for Fe, ≤0.11 wt.% for Cu, 0.05 wt.% for Co and 0.58 wt.% for Ni respectively.

4.4. Laser ablation ICP-MS

Polished blocks were selected for laser ablation inductively coupled plasma mass spectrometry (LA-ICP-MS) for sulphide trace element analysis. Time resolved analysis (TRA) by LA-ICP-MS was performed on each BMS inclusion at Cardiff University on a New Wave Research UP213 UV laser system attached to a Thermo X Series 2 ICP-MS. Each inclusion underwent multiple analyses (by spots, lines, or both) to allow for data repeatability and homogeneity to be assessed (Supplementary Fig. A). Both line and spot analysis were used and independently calibrated. For lines, a minimum length of ~80 μm and a beam diameter of 40 μm were used, with laser operating conditions of 10 Hz frequency, 0.063 mJ at 4.98 J cm^{-2} and sample translation at 6 μm s^{-1}. For spot analysis, beam size was 40 μm and the same laser operating conditions as for the line analyses were employed. Acquisition times ranged from 40 to 80 s with a gas blank measured for 20 s prior to laser ablation. Major element abundances (Fe, Ni, Cu, S) of the sulphide were measured by SEM-EDS (as outlined in Section 4.3) prior to LA-ICP-MS, and ^{33}S was used as an internal standard for trace element calibration. Gas blank subtraction and internal standard corrections were carried out on Thermo Plasmalab software.

Five synthetic Ni-Fe-S quenched sulphide standards were used for LA-ICP-MS calibration, including S, Ni, Fe and Cu as major elements, and Co, As, Se, Ru, Rh, Pd, Ag, Cd, Sb, Te, Re, Os, Ir, Pt, Au and Bi as trace elements. The compositions and details of analytical methods for these standards are presented in Prichard et al. (2013) and further procedural details are available in Smith et al. (2014). Standards 1–3 were used for calibration of Fe, Ni, Cu, Co, Zn and Cd as well as matrix-matched corrections for argide species, which interfere with light PGE isotopes ($^{59}Co^{40}Ar$, $^{61}Ni^{40}Ar$, $^{63}Cu^{40}Ar$, $^{65}Cu^{40}Ar$ and $^{66}Zn^{40}Ar$). Standard 1, containing 143 ppm Cd, was also used in corrections for ^{106}Cd on ^{106}Pd and ^{108}Cd on ^{108}Pd. Independent corrections for isotopes of the same element (e.g., $^{66}Zn^{40}Ar$ and ^{106}Cd on ^{106}Pd, and ^{108}Cd on ^{108}Pd) showed <20% variance for Ru isotopes at concentrations from 0.1–0.2 ppm Ru and 3–10% for Pd isotopes at concentrations around 1 ppm Pd, indicating that the correction criteria are appropriate.

The accuracy for PGE and Au was checked by analysis of the Laflamme-Po724 standard as an unknown against the Cardiff quenched sulphide standards (results in Supplementary Material Table B). Based on the repeated spot and line analyses of each diamond sulphide inclusion (both from the homogenised and unhomogenised sample sets) 1σ precision can be calculated (Table 3). This shows 1σ precision to be typically 3–10% (concentrations 10–100 ppm), 4–41% (1–10 ppm) and 2–46% (<1 ppm) for homogenised samples. All LA-ICP-MS generated data are presented in Table 3, including argide and isobaric-corrected data with values displayed by isotope (for Ru, Rh and Pd).

5. RESULTS

5.1. Sulphide inclusion recovery

Table 1 shows the details of the larger sulphide inclusions recovered in this study. No *whole* inclusions were released from H1, but in total 5 large (>100 μm) and 10 small (<100 μm) pieces were obtained. These were grouped as one population initially. However, single inclusions typically produce 1–5 individual pieces on breakout and as the surface of H1 prevented clear viewing it is highly likely that this collection of fragments represents a mixture derived from a presently unknown number of multiple inclusions. On breakout, all four inclusions originally observed in H2 were recovered virtually whole and the two largest (H2a and H2b) were used for analysis. Diamond H3 shattered on breakout, flaking the one relatively large single inclusion in this stone and the largest fragment (H3a) from this was taken for analysis. Sulphide inclusion H2a (Table 1), had a visibly octahedral shape, imposed by the crystal structure of the diamond. Unhomogenised control diamond inclusions (IM2a, IM2b and IM6a) were recovered as fragments for comparison (Table 1). IM2a and IM2b were two pieces of an originally single inclusion from diamond IM2. IM6a was the largest fragment recovered from a single inclusion contained in stone IM6.

Table 3
Summary table of all trace element data (from LA-ICP-MS) of homogenised and unhomogenised diamond inclusion samples. See main text for details regarding calibration and argide corrections. Refer to supplementary Table B for all certified reference standard data (including all analysed isotopes).

Sample #		Dominant end-member BMS	LOD#	S (stoich)	S (measured)[d]	S/Se[c]	^{57}Fe (wt.%)	^{59}Co (ppm)	^{61}Ni (wt.%)	^{65}Cu (wt.%)	^{75}As (ppm)	^{77}Se (ppm)	^{82}Se (ppm)	^{99}Ru[a] (ppm)	^{101}Ru[a] (ppm)	^{103}Rh[a] (ppm)	^{105}Pd[a] (ppm)	^{106}Pd[a] (ppm)	^{108}Pd[a] (ppm)	^{109}Ag (ppm)	^{111}Cd (ppm)	^{121}Sb (ppm)	^{125}Te (ppm)	^{185}Re (ppm)	^{189}Os (ppm)	^{193}Ir (ppm)	^{195}Pt (ppm)	^{197}Au (ppm)	^{209}Bi (ppm)
Homogenised																													
H1b	H1b line1[b]	n/a	1	38	38.88	6923	55.55	2076	3.41	3.08	<1	-	57	0.155	0.117	0.304	1.00	0.914	0.980	0.260	<0.14	<0.24	2.30	1.30	0.028	0.040	1.01	0.049	0.189
H1b	H1b spot1[b]	n/a	2	38	38.88	6028	55.84	1977	3.35	2.95	<2	-	66	<0.22	<0.14	0.205	1.12	0.991	0.941	0.220	<0.12	0.386	2.43	1.07	0.047	0.077	1.17	0.055	0.160
	Mean					6475	55.69	2027	3.38	3.01			62			0.255	1.06	0.953	0.961	0.240			2.36	1.19	0.038	0.059	1.09	0.052	0.175
	1σ					633	0.21	70	0.04	0.09			6			0.070	0.09	0.055	0.028	0.029			0.091	0.161	0.014	0.027	0.113	0.004	0.020
H1c	H1c line1	n/a	2	38	39.00	2726	53.76	2327	3.47	4.16	<1	147	-	<0.09	<0.05	<0.05	1.04	0.965	1.15	0.853	<0.13	<0.15	2.32	1.31	<0.03	0.088	1.44	0.096	<0.02
H1c	H1c spot1	n/a	3	38	39.00	2682	53.98	2104	3.35	4.05	<1	149	-	<0.09	<0.05	<0.06	1.29	1.36	1.38	0.975	<0.13	<0.15	2.57	1.47	<0.03	0.065	1.93	0.076	0.028
H1c	H1c spot2	n/a	3	38	39.00	2833	54.73	2255	3.47	3.85	<1	141	-	<0.09	<0.05	0.085	1.11	1.04	1.11	0.747	<0.13	<0.15	2.74	1.24	<0.03	0.064	1.02	0.076	<0.02
	Mean					2747	54.16	2229	3.43	4.02		146					1.15	1.12	1.21	0.858			2.54	1.34		0.072	1.46	0.083	
	1σ					77	0.51	114	0.07	0.16		4					0.130	0.213	0.148	0.114			0.213	0.118		0.014	0.453	0.012	
H1d	H1d line1	n/a	2	38	38.82	2632	54.46	2511	3.84	3.44	<1	151	-	0.133	0.149	<0.05	1.12	1.29	1.27	0.273	<0.13	<0.15	5.60	1.12	<0.03	0.053	1.37	0.029	<0.02
H1d	H1d spot1	n/a	3	38	38.82	2752	54.33	2197	3.43	3.55	<1	144	-	0.177	0.150	0.156	1.18	1.13	1.20	0.309	0.346	<0.15	5.69	1.01	<0.03	0.052	1.21	<0.01	<0.02
H1d	H1d spot2	n/a	3	38	38.82	2883	54.51	2162	3.42	3.44	<1	138	-	0.161	0.200	0.105	1.02	1.04	1.22	0.304	<0.13	<0.15	5.06	1.10	<0.03	0.049	1.14	0.016	<0.02
	Mean					2756	54.43	2290	3.56	3.48		144		0.157	0.166	0.130	1.10	1.15	1.23	0.295			5.45	1.08		0.051	1.24	0.023	
	1σ					125	0.09	192	0.24	0.06		7		0.022	0.029	0.037	0.08	0.128	0.038	0.020			0.339	0.062		0.002	0.115	0.009	
H2a	H2a line1	n/a	2	38	39.46	4647	56.93	2478	3.30	1.71	<1	88	-	<0.09	0.080	<0.05	0.08	<0.06	<0.09	0.510	<0.13	<0.15	7.39	0.095	<0.03	<0.02	0.110	0.249	0.032
H2a	H2a spot1	n/a	3	38	39.46	4439	57.20	2243	3.14	1.63	<1	92	-	<0.09	<0.05	<0.06	<0.06	<0.06	<0.09	0.477	<0.13	<0.15	7.50	0.047	<0.03	<0.02	0.202	0.244	<0.02
H2a	H2a spot2	n/a	3	38	39.46	4128	57.30	2412	3.14	1.83	<1	99	-	<0.09	<0.05	<0.06	<0.06	<0.06	0.140	0.665	0.147	<0.15	8.70	0.065	<0.03	<0.02	0.139	0.304	<0.02
	Mean					4405	57.15	2377	3.19	1.72		93								0.551			7.86	0.069			0.150	0.266	
	1σ					261	0.19	121	0.10	0.10		6								0.100			0.727	0.024			0.047	0.033	
H2b	H2b line1[b]	n/a	1	38	39.50	4906	58.06	2196	3.13	1.54	<1	-	84	0.132	0.101	<0.08	<0.13	<0.16	<0.12	0.415	<0.14	<0.24	6.82	0.033	<0.02	<0.02	0.054	0.219	<0.02
H2b	H2b spot1[b]	n/a	2	38	39.50	4619	58.29	2107	3.00	1.33	<2	-	89	<0.22	<0.14	<0.13	<0.14	<0.12	<0.17	0.577	0.201	<0.21	5.91	0.027	<0.03	<0.03	<0.06	0.227	<0.02
H2b	H2b spot2[b]	n/a	2	38	39.50	4943	58.79	2092	3.04	1.43	<2	-	83	<0.22	<0.14	<0.13	<0.14	<0.12	<0.17	0.485	<0.12	<0.21	6.24	0.026	<0.03	<0.03	0.079	0.206	<0.02
	Mean					4823	58.38	2131	3.06	1.43			85							0.492			6.32	0.028			0.066	0.217	
	1σ					178	0.37	56	0.06	0.11			3							0.081			0.460	0.004			0.018	0.011	
H3a	H3a spot1	n/a	3	38	39.08	2609	57.84	1962	1.41	2.24	<1	154	-	<0.09	<0.05	<0.06	<0.06	0.104	0.113	1.02	<0.13	<0.15	3.67	1.45	<0.03	<0.02	0.116	0.089	0.050
H3a	H3a spot2	n/a	3	38	39.08	2896	58.04	1881	1.38	2.25	<1	139	-	<0.09	<0.05	<0.06	<0.06	0.127	<0.09	0.990	<0.13	<0.15	2.95	1.64	<0.03	<0.02	0.210	0.094	0.046
	Mean					2753	57.94	1922	1.39	2.24		146						0.116		1.00			3.31	1.54			0.163	0.092	0.048
	1σ					203	0.14	57	0.03	0.01		11						0.016		0.018			0.504	0.134			0.067	0.003	0.002
Unhomogenised																													
IM2a	IM2a line1	Pn-Mss	2	38	n/a	4556	52.02	2038	8.06	0.94	<1	87	-	<0.09	<0.06	<0.07	0.338	0.306	0.269	1.21	<0.13	<0.17	9.52	0.472	<0.02	<0.02	4.06	0.282	0.230
IM2a	IM2a spot1	Mss	3	38	n/a	4860	55.37	1873	4.37	1.07	0.1	81	-	<0.11	<0.08	<0.10	0.236	0.284	0.317	0.167	<0.16	<0.21	2.61	0.246	<0.02	<0.02	0.166	0.021	<0.05
IM2a	IM2a spot2	Pn-Mss	3	38	n/a	5414	54.68	2214	6.05	1.20	<1	73	-	<0.11	<0.08	<0.10	0.247	0.284	0.289	0.203	<0.16	<0.21	4.84	0.168	<0.02	<0.02	0.253	0.038	<0.05
IM2a	IM2a spot3	Mss	3	38	n/a	4009	56.25	1982	3.72	1.10	<1	98	-	<0.11	<0.08	0.294	0.216	0.199	0.187	0.164	<0.06	<0.21	4.49	0.175	0.032	<0.02	0.227	0.037	0.155
IM2a	IM2a spot4	Cp-Mss	3	38	n/a	5438	47.96	1486	3.63	10.87	1.5	65	-	<0.11	<0.08	<0.10	0.398	0.316	0.350	4.39	<0.16	<0.21	6.31	0.430	<0.02	<0.02	0.370	0.632	<0.05
IM2b	IM2b line1 rim1	Cp-Pn	2	36	n/a	4134	36.69	2007	11.33	14.93	7	69	-	<0.09	<0.06	0.532	1.079	1.119	1.176	13.01	<0.13	0.453	1.28	9.64	<0.02	<0.02	1.71	1.55	<0.05
IM2b	IM2b line1 core	Mss	2	38	n/a	5109	55.99	2299	4.83	0.36	<1	78	-	<0.09	<0.06	<0.07	0.151	0.209	0.186	0.174	<0.13	<0.17	4.69	0.224	0.022	0.030	0.235	0.052	0.177
IM2b	IM2b line1 rim2	Mss	2	37	n/a	5837	52.09	1987	4.24	6.89	<1	69	-	<0.09	<0.06	<0.07	0.206	0.135	0.123	3.60	<0.13	<0.17	0.883	0.600	<0.02	<0.02	0.546	0.494	0.180
IM2b	IM2b line2 all	Cp-Mss	2	37	n/a	3638	46.88	1732	4.87	10.33	<1	82	-	0.198	0.151	0.303	0.223	0.285	0.315	3.11	2.14	<0.17	4.43	1.33	<0.02	0.025	3.14	1.22	0.080
IM2b	IM2b line2 rim1	Cp-Mss	2	36	n/a	5502	40.10	1237	3.74	18.99	<1	70	-	<0.09	<0.06	0.182	2.565	2.227	2.389	4.94	3.22	<0.17	0.493	2.88	<0.02	<0.02	5.46	2.24	<0.05
IM2b	IM2b line2 core	Pn-Mss	2	38	n/a	3679	54.38	2354	6.54	0.38	<1	109	-	0.148	0.221	<0.07	0.351	0.282	0.346	0.191	<0.13	<0.17	5.29	<0.02	0.031	0.051	0.234	0.046	0.175
IM2b	IM2b line2 rim2	Mss	2	38	n/a	5842	54.05	2094	4.50	4.31	<1	69		0.139	0.151	0.524	0.760	0.715	0.640	1.90	0.548	0.471	7.09	0.386	0.030	<0.02	0.971	0.206	0.253
IM2b	IM2b spot1	Pn-Mss	3	38	n/a	5041	53.74	2184	6.24	1.22	<1	79		<0.11	<0.08	<0.10	0.145	0.270	0.218	<0.09	<0.16	<0.21	6.19	0.081	<0.02	<0.02	0.143	<0.01	<0.05
IM2b	IM2b spot2	Pn-Mss	3	38	n/a	4698	53.90	2168	5.46	1.37	<1	85		<0.11	<0.08	<0.10	0.169	0.186	0.181	<0.09	<0.16	<0.21	3.64	0.169	<0.02	<0.02	0.222	0.033	0.124
IM2b	IM2b spot3	Pn-Mss	3	38	n/a	5318	50.04	1762	5.00	5.24	0.1	75		0.118	0.168	<0.10	0.370	0.108	0.204	1.40	<0.06	<0.21	5.13	0.948	<0.02	<0.02	0.187	0.304	0.146
IM2b	IM2b spot4	Mss	3	38	n/a	5974	51.77	1728	4.22	4.78	0.6	67	-	0.149	0.119	<0.10	0.057	0.138	0.166	2.69	<0.16	<0.21	3.91	0.695	<0.02	<0.02	0.267	0.964	<0.05
IM6a	IM6a line1 all	Mss	2	38	n/a	3515	58.24	1855	3.12	1.31	<1	112	-	<0.09	<0.06	<0.07	0.247	0.280	0.280	<0.07	<0.13	<0.17	0.600	<0.02	<0.02	<0.02	0.916	<0.01	<0.05
IM6a	IM6a line1 rim1	Mss	2	38	n/a	4271	52.38	1662	2.80	5.58	<1	92	-	<0.09	<0.06	<0.07	<0.08	<0.08	<0.12	<0.07	<0.13	<0.17	0.354	<0.02	<0.02	<0.02	0.838	<0.01	<0.05
IM6a	IM6a spot1	Mss	3	38	n/a	4087	57.16	2032	3.33	1.06	<1	96	-	<0.11	<0.08	<0.10	0.293	0.335	0.312	<0.09	<0.16	<0.21	3.73	0.088	0.023	0.044	0.442	<0.01	<0.05
IM6a	IM6a spot2	Mss	3	38	n/a	3043	57.82	2098	3.56	1.26	0.8	129	-	<0.11	<0.08	<0.10	0.360	0.299	0.386	<0.09	<0.16	<0.21	6.07	0.099	0.049	0.046	0.448	<0.01	0.053
IM6a	IM6a spot3	Mss	3	38	n/a	3302	55.39	1988	3.94	1.19	0.6	119	-	0.189	0.148	<0.10	0.428	0.427	0.345	<0.09	<0.06	<0.21	4.64	0.075	0.045	0.027	0.490	<0.01	<0.05
IM6a	IM6a spot4	Mss	3	38	n/a	3941	55.50	1995	3.55	1.34	<1	100	-	<0.11	<0.08	<0.10	0.330	0.308	0.285	<0.09	<0.16	<0.21	6.28	<0.02	<0.02	<0.02	0.517	<0.01	0.057
Detection limits (LOD)																													
			1				0.01	0.216	0.01	0.00	1	17	17	0.085	0.046	0.023	0.134	0.164	0.124	0.013	0.142	0.239	0.395	0.014	0.022	0.000	0.034	0.015	0.017
			2				0.01	0.469	0.01	0.01	2	25	25	0.218	0.136	0.038	0.137	0.113	0.171	0.069	0.117	0.207	0.937	0.018	0.036	0.000	0.057	0.038	0.021
			3				0.01	0.135	0.00	0.00	1	3	3	0.075	0.044	0.015	0.060	0.032	0.027	0.045	0.231	0.080	0.607	0.024	0.025	0.000	0.034	0.008	0.008

This means that if the highest S concentration in a homogenised inclusion is 40 wt.%, calculated trace element concentrations would only be ~5% different from those based on the assumed concentration for calibration.

– denotes "isotope not measured".

[a] Denotes isotopes which have been interference-corrected (Standard 1, Cardiff University, matrix matched) for argide species and Cd.

[b] Se concentration based on 82Se isotope for these samples (as opposed to 77Se for all others).

[c] Calculated using measured S abundance (by SEM) and measured Se abundance (by LA-ICPMS)

[d] All homogenised samples were calibrated to measured S abundance (by SEM EDS). Given the larger variation in S abundance for unhomogenised samples (due to presence of end-member BMS), unhomogenised samples were calibrated to a reasonable assumed S abundance of 38 wt.%.

5.2. Petrography and major element mapping

Reflected light microscopy and back-scattered electron (BSE) images by SEM, per polished BMS inclusion, reveals a successful systematic homogenising effect for those diamonds that underwent the experimental heating and quenching process. As can be seen from the example shown in Fig. 4b no zonation in endmember mineralogy can be identified under BSE above a grain size of <1 μm. On the other hand BSE images of unhomogenised samples display multiple sulphide mineral phases with distinct chalcopyrite-rich rims surrounding a pyrrhotite core or sub-solidus re-equilibration textures between pyrrhotite and pentlandite flames with isolated zones of chalcopyrite (Fig. 4a).

Element mapping (by SEM EDS) was also used to visualise the spatial distribution of Fe, Ni and Cu within each inclusion. Distinct zonation is observed for Fe, Ni and Cu at scales of 25–300 μm in the unhomogenised samples (Fig. 4c). With exception of occasional single and multiple pixels that highlight very small (<1 up 3 μm wide) areas of Cu enrichment, but with insufficient Cu to be exsolved chalcopyrite, major elements are uniformly distributed throughout the homogenised inclusions (Fig. 4d). The single bright pixel recorded in the element maps at the bottom of Fig. 4d was found to be a 2 μm wide particle of brass with an identical composition to the SEM sample holder that is present on the surface of the sulphide. It is not part of the sample. No single or multiple pixels (pixel size 0.75 μm) indicating high concentrations of PGE, Re or Au that might represent sulphide containing PGM nanoparticles were observed.

5.3. Micro-CT visualisation

Fig. 5 shows a 3D surface and volume rendering of the μCT data for diamond H3 which contained multiple sulphide inclusions (including several that could not be observed by purely visual means). Volume renderings were generated from discrete scans of the largest of these inclusions, before (Fig. 5b) and after (Fig. 5c) homogenisation. Whilst the diamond has a slightly rounded shape with negative trigons on the residual octahedral faces, the largest inclusion has a distinctive stepped shaped with faces in three inferred directions (x, y, z). This demonstrates that the sulphide inclusion has adopted a negative crystal shape from the diamond host. The definition of this stepped shape is very slightly more rounded for the inclusion *before* homogenisation (Fig. 5b), than *after* homogenisation (Fig. 5c), but this is likely to be an artefact of the resolution limit of the μCT data. For example, the apparent striations in Fig. 5c can result from the slice structure of the tomographic data. Overall, the inclusion shape has been preserved in the homogenised sample indicating that none of

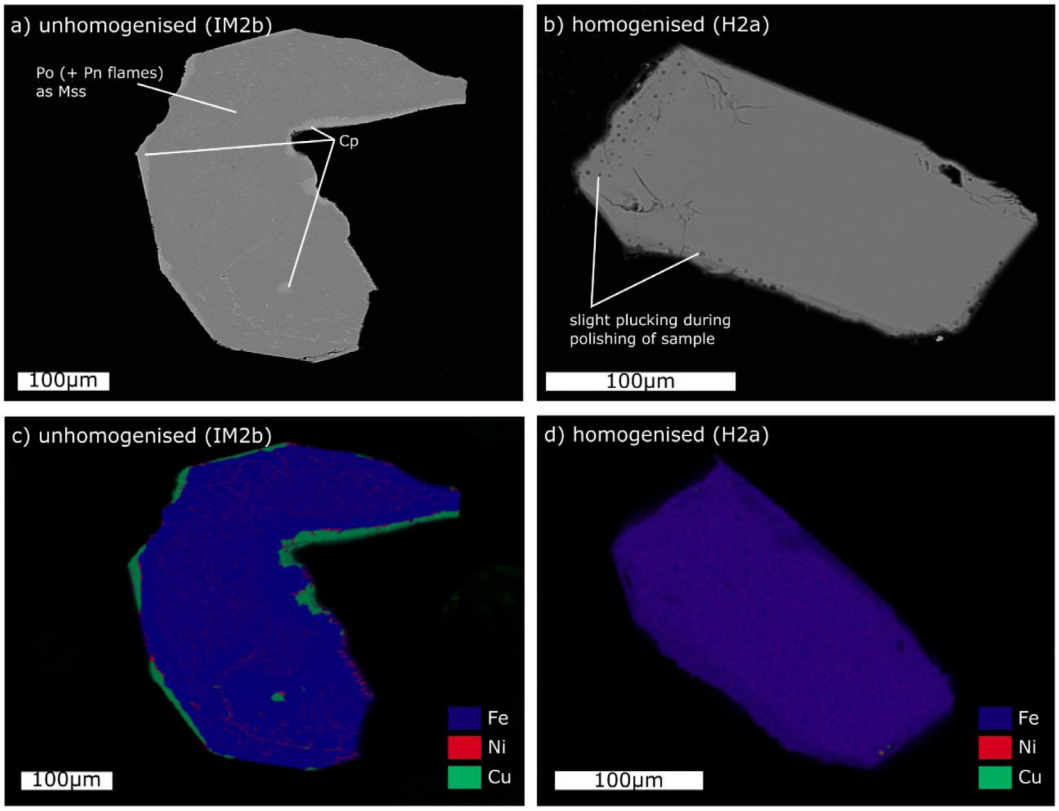

Fig. 4. (a) Back-scattered electron (BSE) scanning electron microscope (SEM) image of unhomogenised inclusion IM2b; (b) BSE-SEM image of homogenised inclusion H2a; (c) combined element maps for Fe, Ni and Cu for unhomogenised inclusion IM2b; (d) combined element maps for Fe, Ni and Cu for homogenised inclusion H2a. Abbreviations are pyrrhotite (Po), pentlandite (Pn), chalcopyrite (Cp) and monosulphide solid solution (Mss).

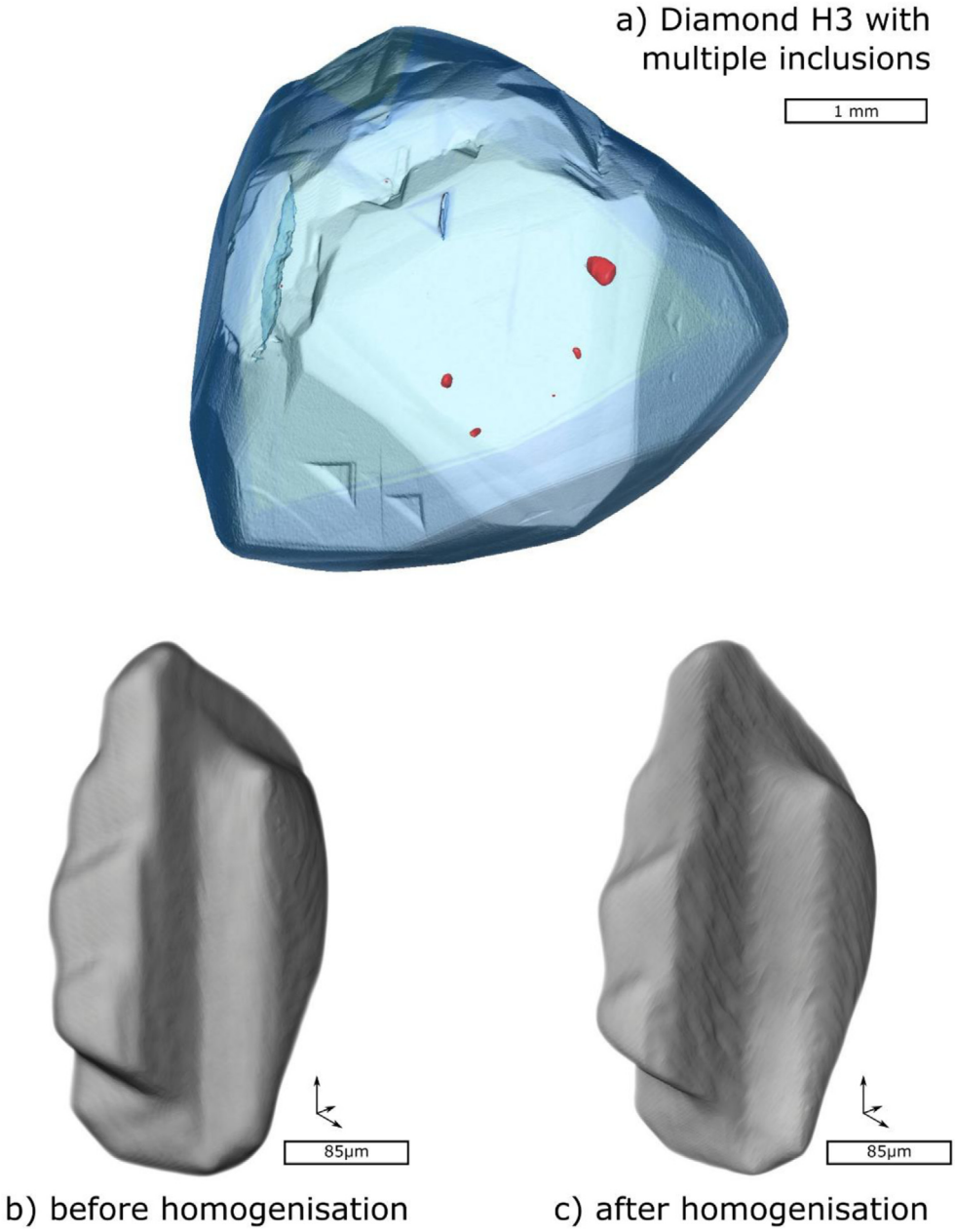

Fig. 5. Micro-CT scan 3D rendered images for diamond H3 and its inclusions. (a) Diamond H3 itself shown as a semi-transparent blue shell with multiple sulphide inclusions as solid red shells. (b) The largest of these sulphide inclusions in H3 before homogenisation and (c) the same inclusion (from the same perspective) after homogenisation. See text for details. (For interpretation of the references to color in this figure legend, the reader is referred to the web version of this article.)

the sulphide material (detectable above the voxel size of 2 μm^3) was lost to fractures or mobilised elsewhere within the diamond.

To determine the volume of the inclusion *before* and *after* homogenisation, the non-local mean-filtered greyscale data were binarised using a global threshold in Avizo 9.2. The total volume of the inclusion was determined from the total voxels in the 3D volume of the binary image and the scan resolution. Before homogenisation the inclusion volume was estimated at 3.31×10^6 μm^3. After homogenisation the inclusion volume was 3.28×10^6 μm^3. Therefore the change in volumes before and after homogenisation are $<1\%$ which was within propagated analytical uncertainty.

Three-dimensional rotating movies of the diamond H3 and its inclusions within (both before and after homogenisation) are available in the online supplementary data files.

5.4. Major element geochemistry

Quantitative major element (S, Fe, Ni, Cu and Co) analyses (by quantitative EDS area analysis) were gathered for each inclusion (or inclusion fragment) for all homogenised

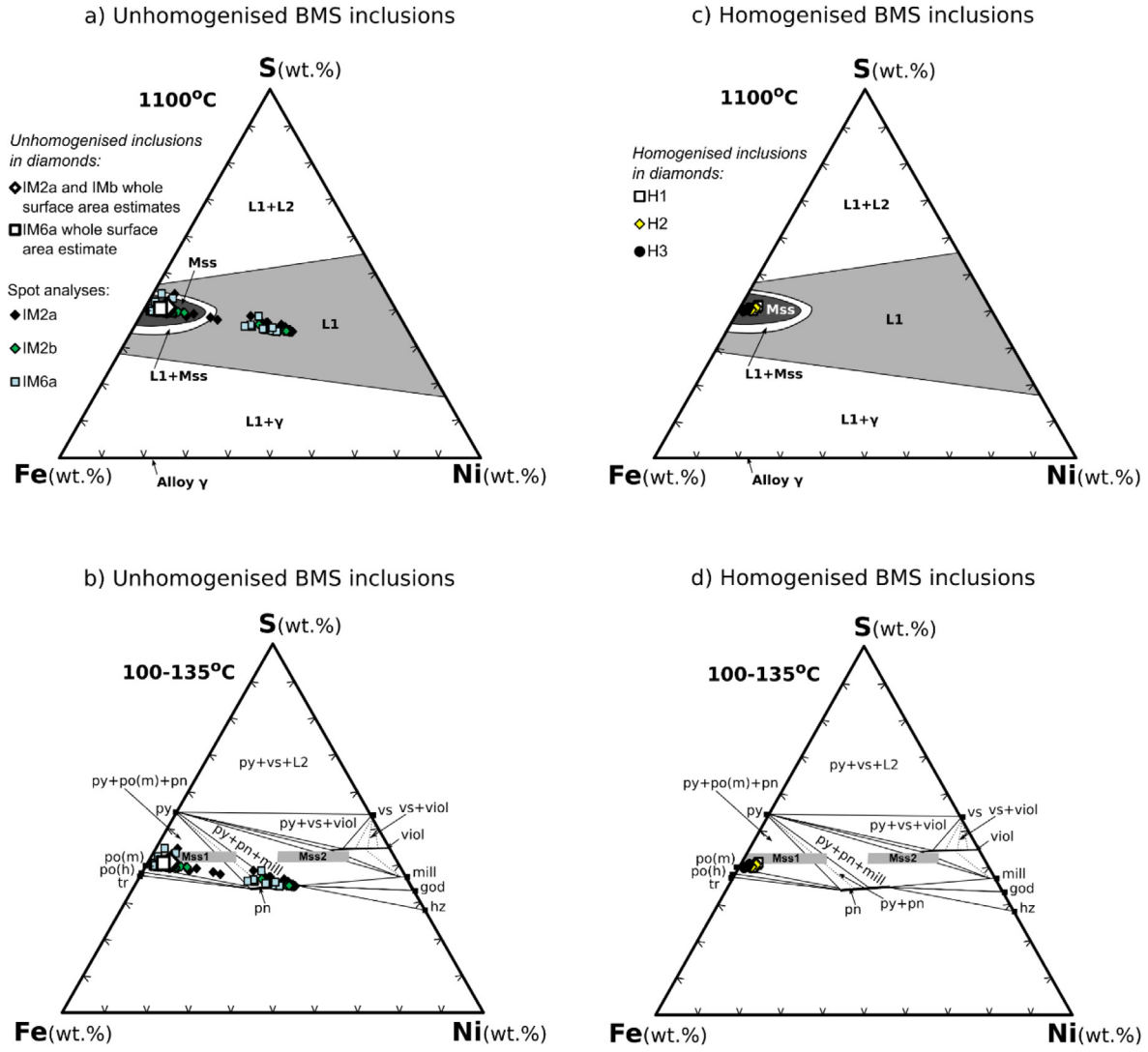

Fig. 6. Ternary Fe-Ni-S diagrams for $T = 1000$ °C and $T = 100$–135 °C. Major element compositions (summarised in Table 2) for unhomogenised samples in (a) and (b). Major element compositions (summarised in Table 2) for homogenised samples in (c) and (d).

and unhomogenised samples in this study (Table 2, *n = 155* – see Supplementary Fig. B). These have been used to establish chemical variability either across single or fragmented sulphides, or between different sulphide fragments from within the same diamond, thereby allowing a quantitative comparison to be made between unhomogenised and homogenised samples. These data are shown in Fig. 6 and a bar chart comparing S, Fe, Ni and Cu abundances by inclusion is given in Supplementary Table C.

The point analyses for the unhomogenised samples ($n = 106$) show a significant degree of variation between endmember compositions (Table 2, Fig. 6a and b). On a ternary Fe-Ni-S compositional diagram projected for a temperature of 1100 °C, these straddle the Mss, Mss + liquid, and liquid (L1) compositional fields (Fig. 6a), and equate to a continuum between pentlandite and pyrrhotite on the 100–135 °C diagram (Fig. 6b). Whilst the data closer to endmember pyrrhotite (Fig. 6b) have some Ni (up to a few wt.%), for pentlandite many analyses plot as endmember compositions. A few analyses (2–5 point data) plot as mixtures between pentlandite and pyrrhotite (due to the spot size on the SEM overlapping fine pentlandite flames within Ni-bearing pyrrhotite). A single 'total' composition (by summing each pixel of the element mapping) based on the whole surface area of each unhomogenised inclusion exposed by polishing, was calculated using the INCA software and shows a representative total assumed composition for IM2 and IM6 (Fig. 6a and b). The calculated 'total' composition for IM2a and IM2b were indistinguishable and were therefore plotted as a single point on these diagrams. These equate to Ni-bearing pyrrhotite compositions akin to those plotted for the homogenised diamonds, but given the nature of the calculation, this alone cannot test the reproducibility of this method in estimating the total composition of an inclusion (as it is dependent upon a single exposed surface).

All analyses for the homogenised samples (*n = 49*) have a comparatively uniform major element composition

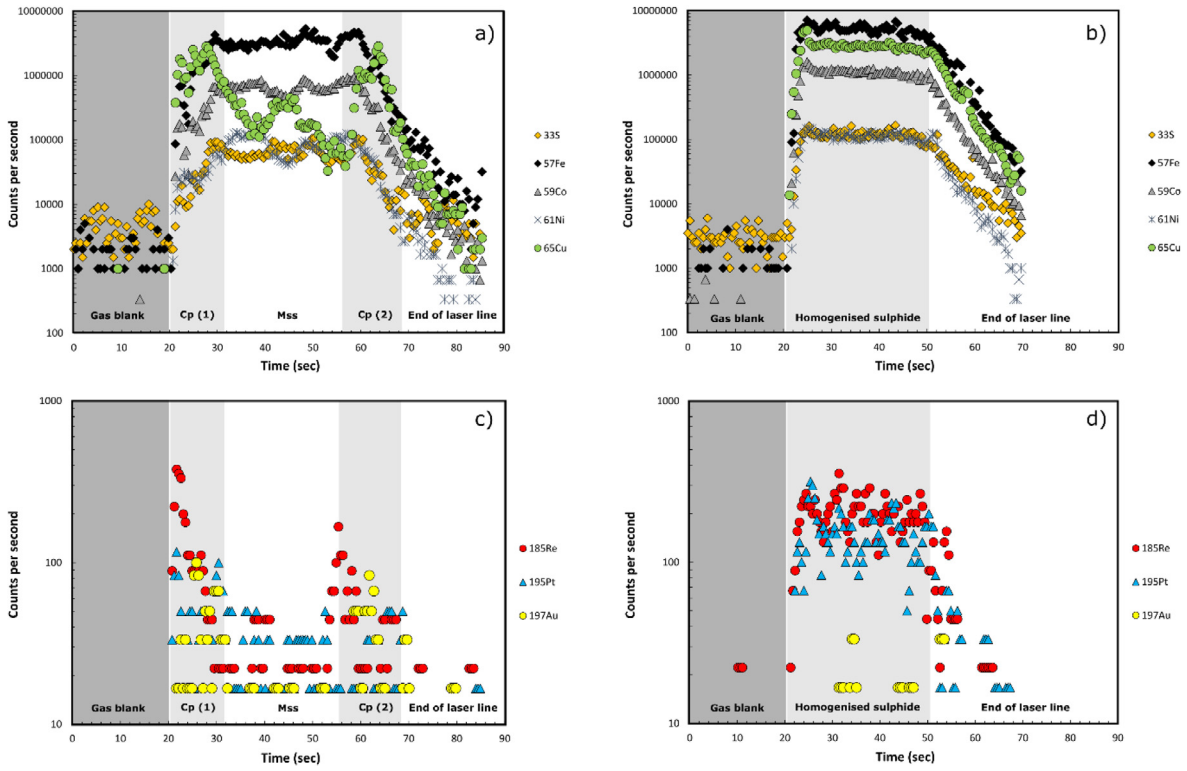

Fig. 7. Time resolved analysis (TRA) spectra for unhomogenised and homogenised inclusions. Major element profiles for (a) unhomogenised inclusion IM2b (line 1) and (b) homogenised inclusion H1d (spot 2). Trace element profiles for (c) unhomogenised inclusion IM2b (line 1) and (d) homogenised inclusion H1d (spot 2).

(Table 2, Fig. 6c and d), with slight but systematic differences between inclusions from different diamonds. Despite appearing homogenous under reflected light and BSE imaging, sulphides from diamond H1 divide into higher and lower Cu populations (H1a and H1c with 3.80 wt.% and H1b and H1d with 3.10 wt.% Cu respectively) that likely reflect at least two different inclusions in the original stone (see Section 5.1). All the H1 sulphides have higher Cu contents and Ni contents than inclusions H2 and H3 (Table 2). In all homogenised inclusions analysed, however, the total Ni content was low enough to prescribe them as being E-type diamonds (<8 wt.% Ni; Yefimova et al., 1983, or <15 wt.% Ni; Deines and Harris, 1995). All of the homogenised sulphide inclusions plot as Ni-bearing pyrrhotite on the ternary Fe-Ni-S compositional diagrams (Fig. 6c and d) and the compositional variation define a very tight data cluster of 42 points plotted on both Fig. 6c and d. Any variation is unresolvable from the natural slight instrument divergence.

5.5. Trace element geochemistry

Representative time resolved analysis (TRA) plots from the LA-ICP-MS data for S, Fe, Ni, Cu and Co indicate that for all the unhomogenised samples, a distinct zonation is noted for major elements, particularly discernible for Cu, an example being shown in Fig. 7a. In all the homogenised samples a zonation cannot be detected (e.g., Fig. 7b). This lack of zonation in the homogenised sulphides extends to the trace elements where important elements like Re and, where measurable, Pt can also be shown to exhibit near uniformity across a sulphide. For example, compare Fig. 7c (unhomogenised) with Fig. 7d (homogenised). These observations are true for both spot and line analyses by LA-ICP-MS. For the homogenised samples, both spot and line analyses give consistent calibrated element abundances (Table 3 and Supplementary Tables B and C). In Table 3 comparisons are given between homogenised trace elements to 1σ values (per isotope analysed for each trace element).

6. DISCUSSION

Before proceeding further it is important to demonstrate that homogenisation has been effective. The BSE-SEM images revealed no phase separation that could be identified above a grain size of <1 μm (Fig. 4) and the element maps only highlighted anomalous Cu-rich pixels on a micron-scale. This is comparable or better than the sulphide homogenisation achieved by Holwell et al. (2011). To further test the homogeneity of major and trace elements we have subdivided the TRA spectra obtained by LA-ICP-MS systematically into 5 s time blocks and determined the counts per second for Fe, Ni, Cu, Se, Ag, Te, Pd, Re, Pt and Au along with ratios (counts/counts) for Fe/Ni, Fe/Cu, Se/Ag, Se/Te, Pt/Pd, Re/Pt and Re/Au in each time block. From multiple time blocks we calculate a mean and standard deviation (1σ) and a relative standard deviation ((σ/mean) × 100%) to represent the variability across

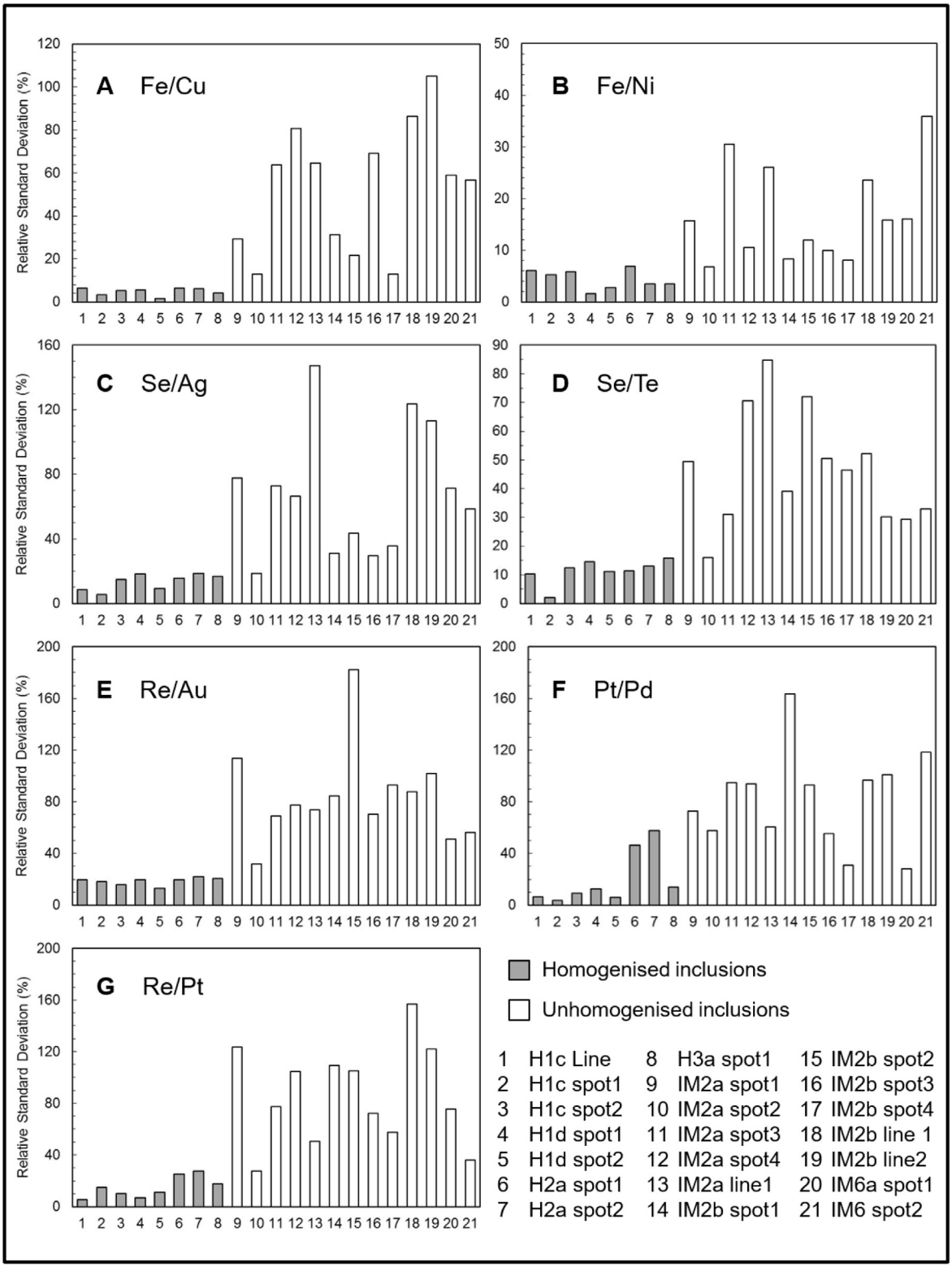

Fig. 8. Comparison of relative standard deviations (%) for elemental ratios in homogenised inclusions (grey bars) and unhomogenised inclusions (open bars). For more information, see text and Supplementary Table D.

the data acquisition. This is shown graphically in Fig. 8 and demonstrates an obvious reduction in variability on these ratios in the homogenised vs the unhomogenised inclusions regardless of whether spots or lines are used for analysis.

In Figs. 9–14 we compare our Orapa sulphide inclusion trace element data with similar comprehensive trace element data for unhomogenised P-type sulphide inclusions from Yakutia (Siberian Craton; Bulanova et al., 1996) and E-type sulphide inclusions from the Diavik Mine (Slave Craton; Aulbach et al., 2012). In addition, the present data are compared against documented Re and Os abundances, from E-type sulphides in diamonds from Jwaneng (Richardson et al., 2004), and Kimberley (Richardson et al., 2001), P-type sulphides in diamonds from Panda (Westerlund et al., 2006) and Yakutia (Wiggers De Vries et al., 2013), P- and E-type sulphide-bearing diamonds from Palmietgat (Simelane, 2004), and sulphides of unspecified paragenesis in diamonds from Swartruggens (McKenna, 2001).

As with the major elements, Time Resolved Analysis (TRA) plots show significant variation in trace elements across single unhomogenised samples. For example, Fig. 7c shows that Re and Au are notably enriched in the Cu-rich portions of the unhomogenised inclusions. By comparison, the homogenised inclusions (see Fig. 7d) shows no such peaked TRA signal for Re, Au or other trace elements. The metal/S ratios (metal = Fe + Ni + Cu) vs PGE abundances, (see Fig. 9a), for all E-type diamonds (this study unhomogenised and homogenised, and similar data from Aulbach et al., 2012), range from 1.50 to 1.82, with total PGE abundances <12 ppm (Fig. 9a). The unhomogenised Orapa sulphide inclusions in that figure show a wide variation in metal/S ratio and total PGE, values reaching up to 1.75 and 8 ppm, with a broadly positive correlation that falls within the range previously documented for Diavik E-type diamonds by Aulbach et al. (2012). The homogenised Orapa inclusions by comparison have a very limited variability (on a diamond-by-diamond basis) giving distinct, but tightly clustering data, as seen in Fig. 9a. Inclusions from homogenised diamond H1, for example, have 2–4 ppm total PGE, an order of magnitude higher than the total PGE concentration of inclusions from diamonds H2 and H3 (0.2–0.4 ppm; see also Table 3). A similar situation exists between unhomogenised and homogenised sulphides if metal-to-metal ratios are compared to the PGEs, as shown in Fig. 9b and c. In these two figures P-type sulphide data are added to allow a comparison with the earlier and present E-type data.

Chondrite normalised Ni-PGE-Au-Re-Cu diagrams (normalised after Fischer-Gödde et al., 2010 for PGE and McDonough and Sun, 1995 for Ni, Re and Cu) are displayed in Fig. 10. The grey background area delineates E-type inclusion compositions from Slave Craton diamonds; Aulbach et al., 2012). Overall, all the Orapa sulphide inclusions analysed in this study have Ni-PGE-Au-Re-Cu patterns similar to those of Aulbach et al. (2012) with IPGE < PPGE. The unhomogenised Orapa inclusion patterns (Fig. 10a) show similar features to the homogenised ones (Fig. 10b), except that variation is minimised in the former. Per diamond, the systematic patterns of homogenised samples are distinct for diamond H1 relative to H2 and H3 (Fig. 10b). For example, Pt, Pd and Re are notably higher in inclusions from diamond H1, and these samples also have a distinctive negative Au anomaly. In compar-

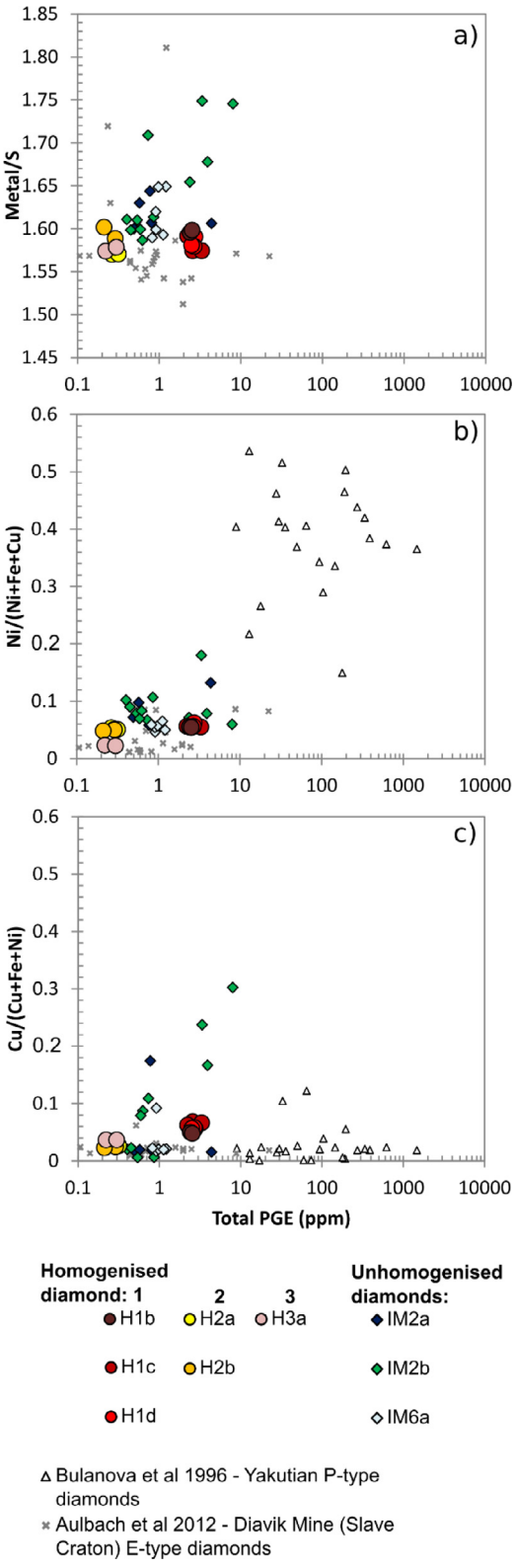

Fig. 9. LA-ICP-MS data for homogenised and unhomogenised inclusions for (a) Metal/S ratio vs total PGE concentration, (b) Ni/(Ni + Fe + Cu) and (c) Cu/(Cu + Fe + Ni). Datasets from Bulanova et al. (1996) and Aulbach et al. (2012) for comparison.

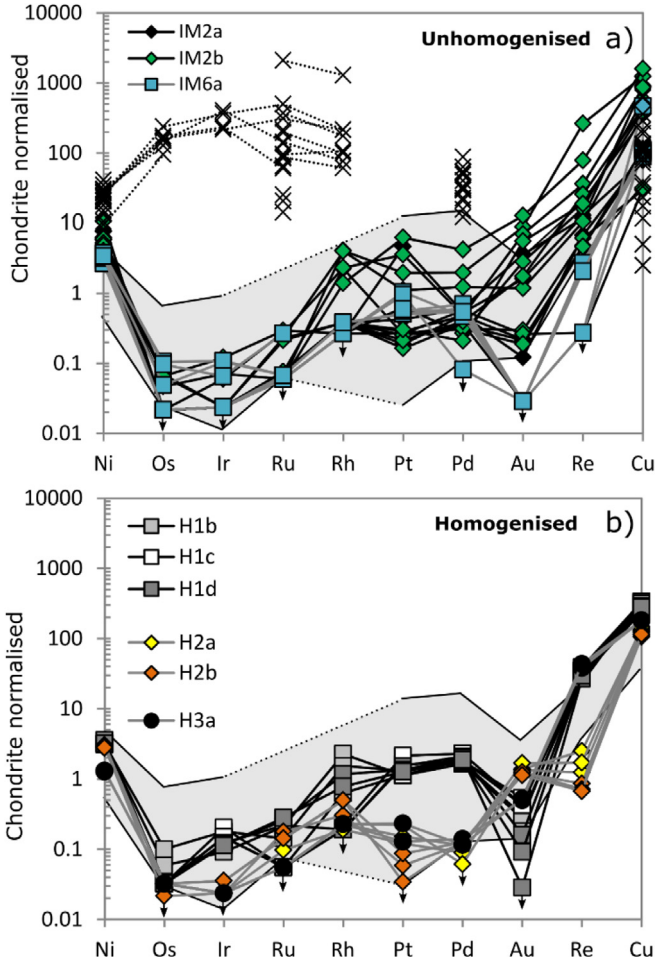

Fig. 10. Multi-element diagrams for Ni, Cu, Re and the PGE: (a) shows unhomogenised samples and (b) shows homogenised samples. The light grey background delineates compositions from Aulbach et al. (2012) E-type Diavik diamond sulphide inclusions whilst the dashed lines indicate P-type diamond compositions from Yakutia by Bulanova et al. (1996). Downward arrows denote measurements where concentration was <LOD, and which have then been plotted at ½LOD.

ison, inclusions from diamonds H2 and H3 have much lower Pt and Pd, slightly lower Os and Ir, a slight positive anomaly for Au and a slightly negative anomaly for Re (Fig. 10b). These apparent diamond-specific variations are not always reconcilable with the unhomogenised samples (Fig. 10a) because the variation from multiple analyses tends to make the pattern more scattered. However, we observed that unhomogenised samples from diamond IM6 have negative Au anomalies and generally the lowest Re concentrations (Fig. 10b). LA-ICP-MS analyses of unhomogenised samples with the highest Cu component appear to have significantly higher Re contents, as well as higher Au, and PPGE (cf. Table 3; Fig. 10b). Also in Fig. 10a, as a series of black crosses associated with some of the Ni-PGE-Au-Re-Cu elements, are patterns for P-type diamonds from the Bulanova et al. (1996) study. These data are clearly distinct, with enriched IPGE (such that IPGE > PPGE), higher Pd and generally lower Cu contents than all the E-type diamonds.

The very low Os abundances in most of the unhomogenised Orapa sulphide inclusions (often < LOD), contrasts with the extreme variation in Re (0.02–9.46 ppm Re; Table 3) in the same sulphide. This relationship causes a spread of $(Re/Os)_N$ values for these samples and is shown in Fig. 11a. By contrast, the $(Re/Os)_N$ variability of homogenised samples, per diamond, is significantly reduced. This variation in unhomogenised samples is proportional to the dominant end-member sulphide mineral selectively sampled by the LA-ICP-MS, and in particular, the $(Re/Os)_N$ ratio is positively correlated with the Cu content (Fig. 11b). Also, very low Ir abundances are observed for most of the analysed Orapa sulphide inclusions (often < LOD), but again the extensive variation in Pd (0.07–2.39 ppm; Table 3) in the unhomogenised samples causes a spread of $(Pd/Ir)_N$ for these samples (see Fig. 11c). This variability is significantly reduced for the homogenised samples.

Fig. 11d shows that the limited number of P-type sulphide-bearing diamonds analysed to date by Bulanova et al. (1996) have very low $(Pd/Ir)_N$ relative to the E-type diamond dataset. This separation is largely controlled by the high Ir contents of the P-type diamonds, and the low to very low (<LOD) Pd contents. Consequently, the

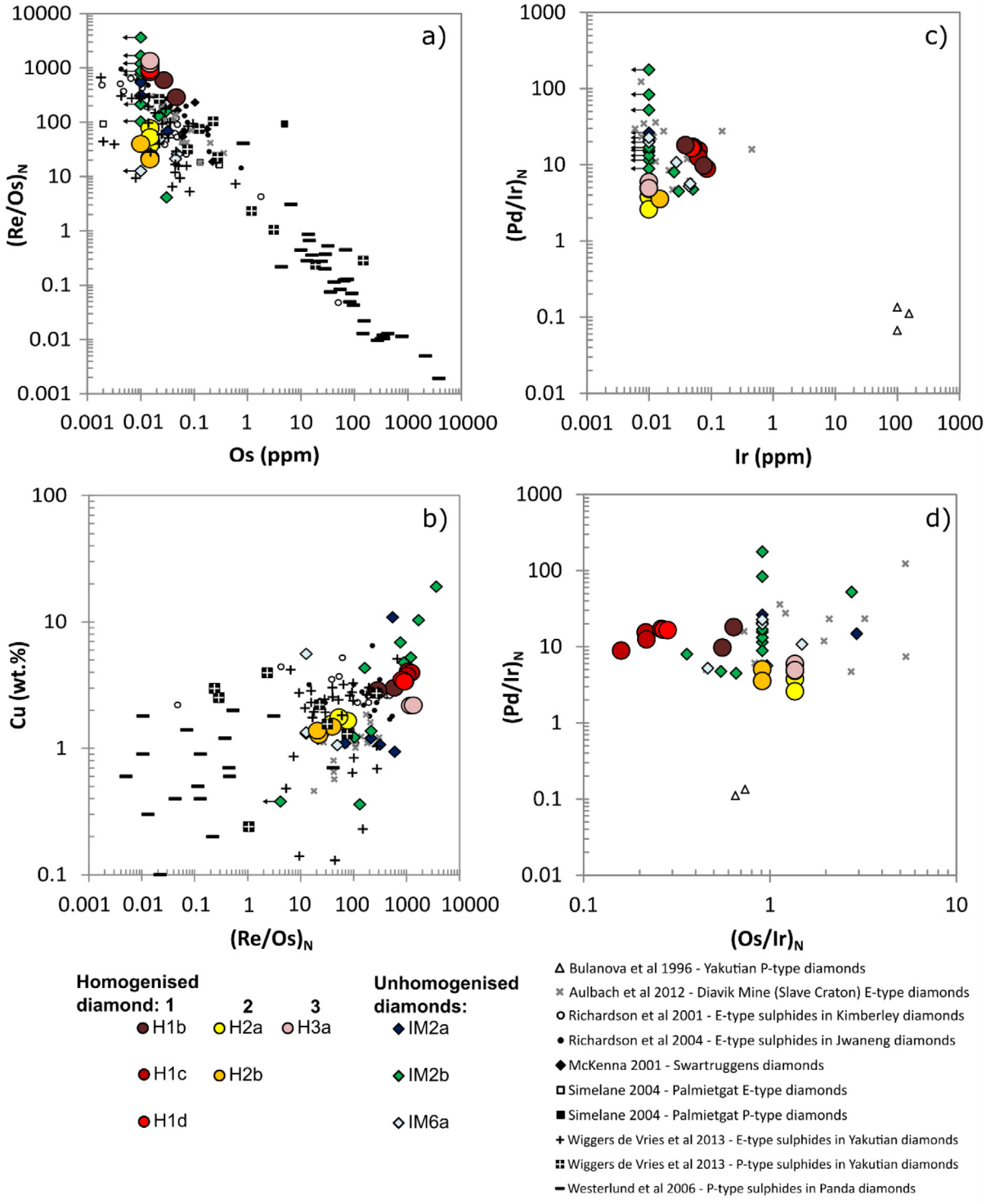

Fig. 11. LA-ICP-MS data for homogenised and unhomogenised inclusions for (a) $(Re/Os)_N$ vs Os, (b) $(Re/Os)_N$ vs Cu, (c) $(Pd/Ir)_N$ vs Ir and (d) $(Pd/Ir)_N$ vs $(Os/Ir)_N$ compared with literature data. Data sources: P-type sulphides (Bulanova et al., 1996; Simelane, 2004; Westerlund et al., 2006; Wiggers de Vries et al., 2013); E-type sulphides (Richardson et al., 2001, 2004; Simelane, 2004; Aulbach et al., 2012); unknown paragenesis (McKenna, 2001). Downward arrows denote measurements where concentration was <LOD, and which have then been used at ½LOD for calculated ratios for plotting.

E- and P-type sulphide inclusions fall in distinct areas on $(Pd/Ir)_N$ vs $(Os/Ir)_N$ diagrams, (see Fig. 11d). More analyses of P-type sulphides from a greater number of localities will be needed to establish the true extent of this separation.

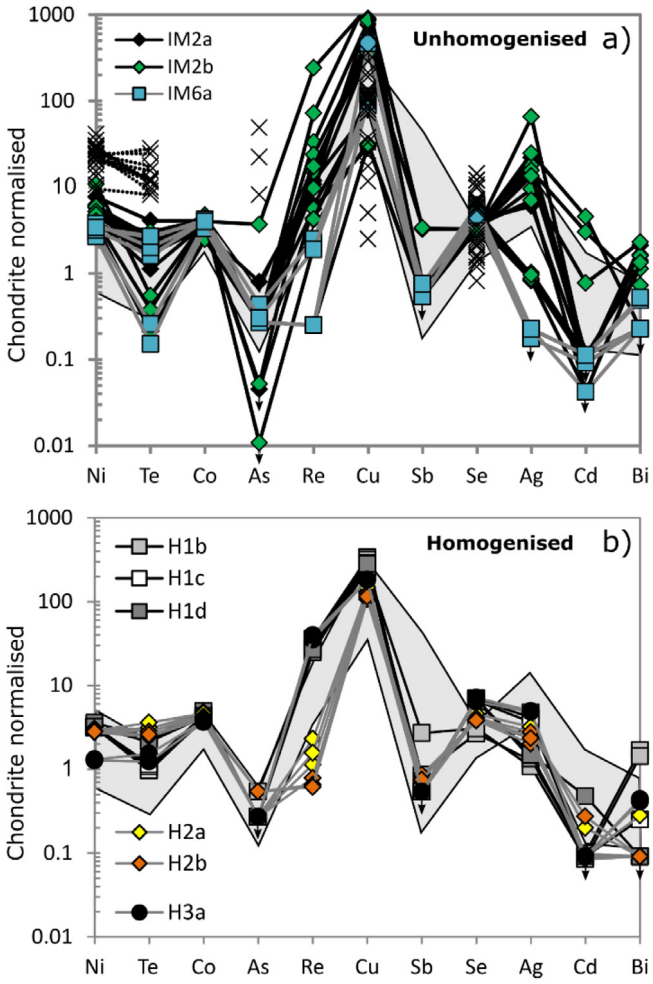

Fig. 12. Multi-element diagrams for semi-metals and major elements: (a) shows unhomogenised samples and (b) shows homogenised samples. The light grey background delineates compositions from Aulbach et al. (2012) E-type Diavik diamond sulphide inclusions whilst the crosses and dashed lines indicate Yakutian P-type diamond compositions from Bulanova et al. (1996). The order of elements in these diagrams is based on Aulbach et al. (2012). Downward arrows denote measurements where concentration was <LOD, and which have then been plotted at ½LOD.

Chondrite normalised (after McDonough and Sun, 1995) multi-element diagrams for semi-metals and base metals are shown in Fig. 12 (with the light grey area delineating the compositional range of the E-type sulphide inclusions from Aulbach et al. (2012)). Again, a greater variation in compositions is seen for the unhomogenised samples in Fig. 12a than for the homogenised Orapa inclusion samples of Fig. 12b. All E-type BMS inclusions observed have slight negative and slight positive anomalies for Te and Co, respectively, with unhomogenised samples having a particularly wide spread in Te abundance (Fig. 12a). All E-type BMS inclusions also have a notable negative As anomaly. Antimony, Ag, Cd and Bi are very variable between unhomogenised samples from different diamonds. For the homogenised diamond suite, H1 has the highest Bi content and generally (although not uniformly) the lowest Cd. Conversely, the P-type diamonds shown as black crosses in Fig. 12a are distinctive from the E-type compositions, with notably higher Te and As, and a great spread in Se abundances.

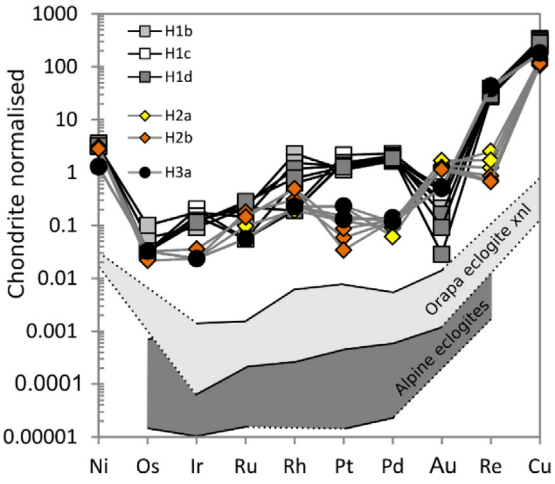

Fig. 13. Multi-element diagrams for Ni, Cu, Re and the PGE comparing homogenised diamond inclusion samples with bulk rock data for eclogite xenoliths, abbreviated 'xnl', from Orapa (McDonald and Viljoen, 2006) and for Alpine eclogites (Dale et al., 2009).

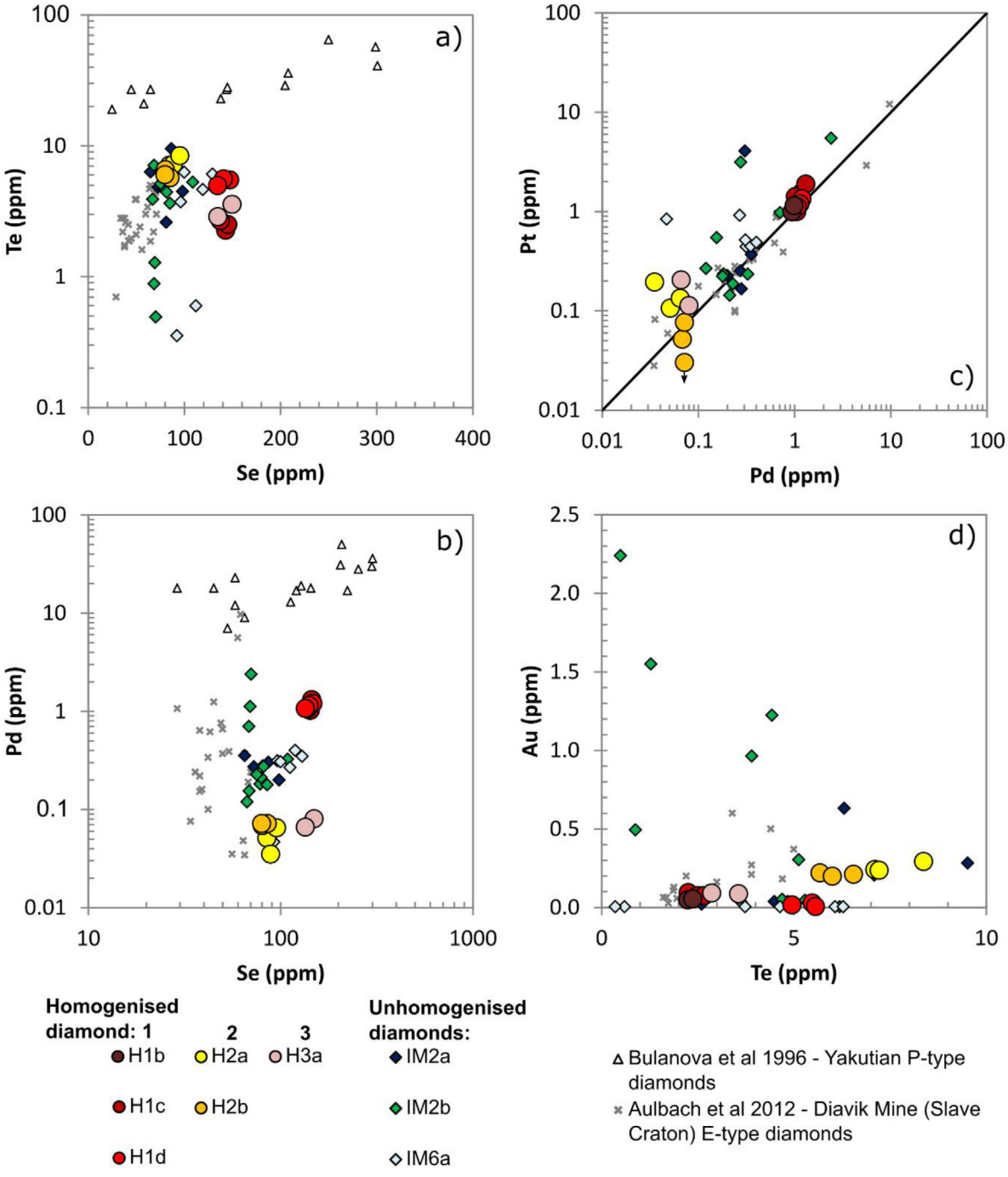

Fig. 14. LA-ICP-MS data for homogenised and unhomogenised inclusions for (a) Te vs Se, (b) Pd vs Se, (c) Pt vs Pd and (d) Au vs Te.

7. WIDER IMPLICATIONS

7.1. Comparisons with whole E-type diamonds and whole rock eclogites

Hart et al. (1997) determined Au and Ir concentrations in whole diamonds and found that their E-type diamond data formed a steep and positively sloped array on a Au vs Ir plot with Au/Ir ratios > 0.3, whereas their P-type diamonds generally formed a cluster of data with Au/Ir < 0.3 (Supplementary Fig. C). In both cases, absolute metal concentrations were very low (<0.01 ppm) as the Au and Ir-bearing phases were diluted by the larger mass of the host diamond. The data generated in this present sulphide inclusion study and that of Aulbach et al. (2012) plot as an extension of the earlier E-type diamond Au vs Ir array (Supplementary Fig. C) and confirm that the Au and PGE concentrations in a whole diamond are probably controlled by small BMS inclusions. Such inclusions would be sub-microscopic in the case of diamonds that appear to be visually clear.

McDonald and Viljoen (2006) measured PGE and Au concentrations in whole rock samples of eclogites from

Orapa and these are compared with alpine eclogites (Dale et al., 2009) and the homogenised BMS inclusions from this study on a chondrite normalised element plot in Fig. 13. The whole rock Orapa eclogites show moderate fractionation of PPGE over IPGE and strong Cu enrichment. Rhenium was not measured in the Orapa eclogite rocks but was in the alpine eclogites. The alpine eclogites generally have lower PGE concentrations but similar pattern shapes to the Orapa eclogites and also show a strong enrichment in Re. The metal concentrations of the E-type sulphide inclusions are 2–3 orders of magnitude greater than the eclogite whole rock samples, but they show similar PPGE:IPGE fractionation and the enrichment in Re and Cu observed in the whole rocks. Comparison of the sulphide inclusion BMS to the bulk rock eclogite data suggests that the PGE and Cu budget is largely controlled by the BMS compositions within the eclogites, however the Re concentration in some of the diamond BMS inclusions is slightly lower than is predicted by the eclogite bulk rock geochemistry. This may be specific to the diamond BMS inclusions analysed during this study, or it may indicate a non-BMS Re-bearing phase such as garnet or talc present within the eclogite xenoliths but absent in some of the diamond BMS inclusions (Dale et al., 2009).

7.2. Precious and semi-metal content of E-type vs P-type diamond sulphide inclusions

The precious and semi-metal contents of E- and P-type diamond BMS inclusions appear to define entirely distinct compositions. E-type BMS generally have low PGE abundances, with PPGE enriched above IPGE, generally lower Se contents, and systematically lower Te and As concentrations than P-type diamond BMS inclusions. E-type BMS also have higher metal/S ratios, lower Ni contents and higher and/or more variable Cu contents. Re concentrations between E- and P-type BMS largely overlap (e.g. Westerlund et al., 2006), however the notably higher Os abundance in P-type BMS inclusions produces a significant difference in $(Re/Os)_N$ ratios.

Fig. 14a shows that Te is higher in all P-type sulphide inclusions (Bulanova et al., 1996) than E-type inclusions (this study and Aulbach et al., 2012) and there is a distinctive positive correlation between Te and Se for P-type inclusions that is absent for E-type. P-type inclusions also have distinctly higher Pd contents than E-type, such that the two populations of diamond inclusion types follow different trends in Fig. 14b (increasing Pd content with increasing Se for P-type inclusions only). Platinum was generally < LOD in the Bulanova study and therefore we cannot compare Pt/Pd ratios for P- and E-type inclusions, however we note that all E-type inclusions fall along a Pt:Pd line close to unity (Fig. 14c), and this trend is observed for inclusions from different host diamonds. Gold and Te do not correlate with one another in the unhomogenised inclusions, nor in the dataset of Aulbach et al. (2012), see (Fig. 14d). But when homogenised, 5 out of the 6 Orapa inclusions define positive a trend between Au and Te. This suggests that Au and Te may be irregularly distributed within or between sulphide minerals (possibly as intermetallic minerals or micro-nuggets) that can be recombined by homogenisation.

In all diagrams in Fig. 14, the homogenised inclusions form a tight cluster of compositions and therefore are much less compositionally variable than analyses of the unhomogenised samples. Whilst the homogenised inclusions tend to cluster per diamond host, we note that the two inclusions from diamond H2 (which existed as two distinct inclusions within the diamond *before* homogenisation, and remained as such *after* homogenisation) have different element concentrations – inclusion H2a has higher Cu, Se, Re, Te and Pt contents than H2b (Fig. 14c) and this is likely to be a primary feature inherited when each BMS inclusion was encapsulated. The same is probably true for the fragments from diamond H1. H1a and H1c have higher Cu than H1b and H1d (Table 2). The different S/Se ratios, Te, Au and Bi concentrations further suggest that each of the large fragments represented by H1b, H1c and H1d originally came from separate inclusions rather than one inclusion as originally suspected.

This intrinsic difference in metallogenic budgets evidenced by E- and P-type diamond BMS inclusions may have significant implications for the metallogenesis of the lithospheric mantle and/or the sources of metals in mantle-derived melts (e.g., Saunders et al., 2015; Hughes et al., 2015, 2017). Figs. 10–12 reveal surprisingly close similarities between the semi-metals present in E-type sulphides from Orapa and Diavik despite the diamonds and sulphides forming on different cratons. This may reflect common protoliths or petrogenetic processes operating during the formation of eclogites and their diamonds on the Slave and Kalahari cratons. Comparison of homogenised E- and P-type diamond BMS inclusions presents an opportunity to assess the wider metallogeny of the two main endmember lithologies of the mantle whilst removing uncertainties over secondary modification. Such studies may have major implications for the metal budget of mantle-derived melts in various tectonic environments through space and time and with metals transport during the formation and evolution of diamond.

8. CONCLUSIONS

- Heating diamonds (intact) with their inclusions in a furnace at 1100 °C, for 15 min under controlled fO_2 conditions followed by quenching, successfully homogenises BMS inclusion(s), eradicating distinct endmember sulphide minerals (formed during natural cooling via subsolidus exsolution processes).
- μCT scanning of the diamond confirms that inclusions are the same volume (within error) both *before* and *after* homogenisation, demonstrating the success of this method. The diamond host retains each BMS inclusion with no loss or gain of inclusion material.
- μCT methods also give an effective insight into the shape of BMS inclusions, including fracture propagation within diamond hosts. In this study, we observe a distinctive 3D stepped shape of a BMS inclusion and suggest this is in the form of a negative crystal shape, invoked by the diamond host.

- This homogenisation method produces BMS inclusions of a uniform geochemical composition for both major and trace elements (per inclusion). This has three implications:
  - o Multiple geochemical analyses may now be carried out on homogeneous fragments of a single BMS inclusion, allowing for complimentary data (e.g., radiogenic and stable isotope systematics, age determinations and trace element characteristics) to be generated from progressively smaller amounts of the same sample.
  - o Concerns regarding missing Re-rich mineral phases from unhomogenised BMS inclusions (e.g., by 'flaking' of chalcopyrite and accidental incomplete sampling of whole inclusions) can be eradicated by utilising this homogenisation method.
  - o If multiple inclusions occur within a single diamond, each may be analysed individually to assess spatial variation of BMS composition in a single diamond.

- Comparison of E-type diamond BMS inclusions in diamond to whole rock eclogite compositions for PGE, Re, Au and Cu indicate that all metals (with the possible exception of Re) are accounted for by the BMS.
- E-type and P-type diamond BMS inclusions in diamond have distinct trace element signatures, especially for precious, heavy and semi-metals. P-type BMS inclusions have higher total PGE and Te concentrations, higher IPGE (Os, Ir and Ru) and As abundances than E-type BMS inclusions. This has important implications for Earth's long term carbon cycle, the metallogeny of the mantle, the partitioning behaviour of trace metals during partial melting, and the metal budgets that may be imparted into mantle-derived magmas.

ACKNOWLEDGEMENTS

HSRH gratefully acknowledges her current Postdoctoral Fellowship with the Claude Leon Foundation and the support of the CIMERA centre of excellence at the Universities of the Witwatersrand and Johannesburg. The Diamond Trading Company (a member of the DeBeers Group of Companies) is thanked for the donation to JWH of the diamonds used in this study. The analytical work in this study was supported by NERC SoS Consortium grant NE/M011615/1 "Te and Se Cycling and Supply" awarded to Cardiff University. The authors would like to thank Associate Editor Amy Riches and the three anonymous reviewers for their advice and comments that significantly improved the paper.

APPENDIX A. SUPPLEMENTARY MATERIAL

Supplementary data associated with this article can be found, in the online version, at http://dx.doi.org/10.1016/j.gca.2017.04.039.

REFERENCES

Agrosì G., Nestola F., Tempesta G., Bruno M., Scandale E. and Harris J. (2016) X-ray tomographic study of a diamond from Udachnaya: implications for the genetic nature of inclusions. *Lithos* **248**, 153–159.

Arnold R. G. (1971) Evidence for liquid immiscibility in the system FeS-S. *Econ. Geol.* **66**(8), 1121–1130.

Aulbach S., Stachel T., Seitz H. M. and Brey G. P. (2012) Chalcophile and siderophile elements in sulphide inclusions in eclogitic diamonds and metal cycling in a Paleoproterozoic subduction zone. *Geochim. Cosmochim. Acta* **93**, 278–299.

Barnes S. J., Makovicky E., Makovicky M., Rose-Hansen J. and Karup-Moller S. (1997) Partition coefficients for Ni, Cu, Pd, Pt, Rh, and Ir between monosulfide solid solution and sulfide liquid and the formation of compositionally zoned Ni-Cu sulfide bodies by fractional crystallization of sulfide liquid. *Can. J. Earth Sci.* **34**(4), 366–374.

Bowles J. F. W., Howie R. A., Vaughan D. J. and Zussman J. (2011) Rock-forming Inerals: Non-silicates: Oxides, Hydroxides and Sulphides. Geological Society.

Bulanova G. P. (1995) The formation of diamond. *J. Geochem. Explor.* **53**(1), 1–23.

Bulanova G. P., Griffin W. L., Ryan C. G., Shestakova O. Y. and Barnes S. J. (1996) Trace elements in sulfide inclusions from Yakutian diamonds. *Contrib. Miner. Petrol.* **124**(2), 111–125.

Burgess R., Kiviets G. B. and Harris J. W. (2004) Ar–Ar age determinations of eclogitic clinopyroxene and garnet inclusions in diamonds from the Venetia and Orapa kimberlites. *Lithos* **77**(1), 113–124.

Carlson R. W. (2005) Application of the Pt–Re–Os isotopic systems to mantle geochemistry and geochronology. *Lithos* **82**(3), 249–272.

Chaussidon M., Albarede F. and Sheppard M. F. (1987) Sulphur isotope heterogeneity in the mantle from ion microprobe measurements of sulphide inclusions in diamonds. *Nature* **330**, 242–244.

Dale C. W., Burton K. W., Pearson D. G., Gannoun A., Alard O., Argles T. W. and Parkinson I. J. (2009) Highly siderophile element behaviour accompanying subduction of oceanic crust: whole rock and mineral-scale insights from a high-pressure terrain. *Geochim. Cosmochim. Acta* **73**, 1394–1416.

Damarupurshad A., Hart R., Sellschop J. and Meyer H. (1997) The application of INAA to the geochemical analysis of single diamonds. *J. Radioanal. Nucl. Chem.* **219**(1), 33–39.

Dasgupta R. and Hirschmann M. M. (2010) The deep carbon cycle and melting in Earth's interior. *Earth Planet. Sci. Lett.* **298**, 1–13.

Davis D. L. (1977) The ages and Uranium contents from kimberlites and associated rocks. In *Extended Abstracts of the Second International Kimberlite Conference, Santa Fe*.

Deines P. (1974) Temperature-oxygen Fugacity Tables for Selected Gas Mixtures in the System CHO at One Atmosphere Total Pressure. College of Earth and Mineral Sciences, Pennsylvania State Univ..

Deines P. and Harris J. W. (1995) Sulfide inclusion chemistry and carbon isotopes of African diamonds. *Geochim. Cosmochim. Acta* **59**(15), 3173–3188.

Eldridge C. S., Compston W., Williams I. S., Harris J. W. and Bristow J. W. (1991) Isotope evidence for the involvement of recycled sediments in diamond formation. *Nature* **353**(6345), 649–653.

Farquhar J., Wing B. A., McKeegan K. D., Harris J. W., Cartigny P. and Thiemens M. H. (2002) Mass-independent sulfur of inclusions in diamond and sulfur recycling on early Earth. *Science* **298**(5602), 2369–2372.

Fesq H., Bibby D., Sellschop J. and Watterson J. (1973) The determination of trace-element impurities in natural diamonds by instrumental neutron activation analysis. *J. Radioanal. Nucl. Chem.* **17**(1–2), 195–216.

Fesq H. W., Bibby D. M., Erasmus C. S., Kable E. J. D. and Sellschop J. P. F. (1975) A comparative trace element study of diamonds from Premier, Finsch and Jagersfontein mines, South Africa. *Phys. Chem. Earth* **9**, 817–836.

Fischer-Gödde M., Becker H. and Wombacher F. (2010) Rhodium, gold and other highly siderophile element abundances in chondritic meteorites. *Geochim. Cosmochim. Acta* **74**, 356–379.

Fleet M. E., Stone W. E. and Crocket J. H. (1991) Partitioning of palladium, iridium, and platinum between sulfide liquid and basalt melt: effects of melt composition, concentration, and oxygen fugacity. *Geochim. Cosmochim. Acta* **55**(9), 2545–2554.

Fleet M. E., Chryssoulis S. L., Stone W. E. and Weisener C. G. (1993) Partitioning of platinum-group elements and Au in the Fe–Ni–Cu–S system: experiments on the fractional crystallization of sulfide melt. *Contrib. Miner. Petrol.* **115**(1), 36–44.

Haggerty S. E., Raber E. and Naeser C. W. (1983) Fission track dating of kimberlitic zircons. *Earth Planet. Sci. Lett.* **63**(1), 41–50.

Harris J. and Gurney J. J. (1979) Inclusions in diamond. In *The Properties of Diamond*, pp. 555–591.

Hart R. J., Tredoux M. and de Wit M. J. (1997) Refractory trace elements in diamond inclusions: further clues to the origins of the ancient cratons. *Geology* **25**(12), 1143–1146.

Harvey J., Warren J. M. and Shirey S. B. (2016) Mantle sulfides and their role in Re-Os and Pb isotope geochronology. *Rev. Mineral. Geochem.* **81**(1), 579–649.

Helmy H. M., Ballhaus C., Berndt J., Bockrath C. and Wohlgemuth-Ueberwasser C. (2007) Formation of Pt, Pd and Ni tellurides: experiments in sulfide–telluride systems. *Contrib. Miner. Petrol.* **153**(5), 577–591.

Holwell D. A. and McDonald I. (2010) A review of the behaviour of platinum group elements within natural magmatic sulfide ore systems. *Platin. Met. Rev.* **54**(1), 26–36.

Holwell D. A., McDonald I. and Butler I. B. (2011) Precious metal enrichment in the Platreef, Bushveld Complex, South Africa: evidence from homogenized magmatic sulfide melt inclusions. *Contrib. Miner. Petrol.* **161**(6), 1011–1026.

Hughes H. S., McDonald I. and Kerr A. C. (2015) Platinum-group element signatures in the North Atlantic Igneous Province: implications for mantle controls on metal budgets during continental breakup. *Lithos* **233**, 89–110.

Hughes H. S., McDonald I., Loocke M., Butler I. B., Upton B. G. and Faithfull J. W. (2017) Paradoxical co-existing base metal sulphides in the mantle: the multi-event record preserved in Loch Roag peridotite xenoliths, North Atlantic Craton. *Lithos* **276**, 103–121.

Kullerud G. and Yoder H. S. (1959) Pyrite stability relations in the Fe-S system. *Econ. Geol.* **54**(4), 533–572.

Luguet A. and Reisberg L. (2016) Highly siderophile element and ^{187}Os signatures in non-cratonic basalt-hosted peridotite xenoliths: Unravelling the origin and evolution of the post-archean lithospheric mantle. *Rev. Mineral. Geochem.* **81**, 305–367.

McCourt S., Kampunzu A. B., Bagai Z. and Armstrong R. A. (2004) The crustal architecture of Archaean terranes in Northeastern Botswana. *S. Afr. J. Geol.* **107**, 147–158.

McDonald I. and Viljoen K. S. (2006) Platinum-group element geochemistry of mantle eclogites: a reconnaissance study of xenoliths from the Orapa kimberlite, Botswana. *Appl. Earth Sci.* **115**, 81–93.

McDonald I., Harris J. W. and Vaughan D. J. (1996) Determination of noble metals in sulphide inclusions from diamonds using inductively coupled plasma-mass spectrometry. *Anal. Chim. Acta* **333**(1), 41–49.

McDonough W. F. and Sun S. (1995) The composition of the Earth. *Chem. Geol.* **120**, 223–253.

McKenna N. (2001) A study of the diamonds, diamond inclusion minerals and other mantle minerals from the Swartruggens kimberlite, South Africa MSc thesis. University of Cape Town, 226p.

Meyer H. O. (1987) Inclusions in diamond. *Mantle xenoliths* **1**, 501–522.

Mungall J. E., Andrews D. R., Cabri L. J., Sylvester P. J. and Tubrett M. (2005) Partitioning of Cu, Ni, Au, and platinum-group elements between monosulfide solid solution and sulfide melt under controlled oxygen and sulfur fugacities. *Geochim. Cosmochim. Acta* **69**(17), 4349–4360.

Naldrett A. J. (1989) Sulfide melts; crystallization temperatures, solubilities in silicate melts, and Fe, Ni, and Cu partitioning between basaltic magmas and olivine. *Rev. Econ. Geol.* **4**, 5–20.

Naldrett A. J. (2011) Fundamentals of magmatic sulfide deposits. *Rev. Econ. Geol.* **17**, 1–50.

Nestola F., Jung H. and Taylor L. A. (2017) Mineral inclusions in diamonds may be synchronous but not syngenetic. *Nat. Commun.* **8**.

Pearson D. G., Shirey S. B., Harris J. W. and Carlson R. W. (1998) Sulphide inclusions in diamonds from the Koffiefontein kimberlite, S Africa: constraints on diamond ages and mantle Re–Os systematics. *Earth Planet. Sci. Lett.* **160**(3), 311–326.

Prichard H. M., Knight R. D., Fisher P. C., McDonald I., Zhu M.-F. and Wang C. Y. (2013) Distribution of platinum-group elements in magmatic and altered ores in the Jinchuan intrusion, China: an example of selenium remobilization by postmagmatic fluids. *Miner. Deposita* **48**, 767–786.

Richardson S. H. (1989) Radiogenic isotope studies of diamond inclusions. In *28th Intl. Geol. Congress, Workshop on Diamonds. Extended Abstracts*, pp. 87–90.

Richardson S. H., Shirey S. B., Harris J. W. and Carlson R. W. (2001) Archean subduction recorded by Re–Os isotopes in eclogitic sulfide inclusions in Kimberley diamonds. *Earth Planet. Sci. Lett.* **191**(3), 257–266.

Richardson S. H., Shirey S. B. and Harris J. W. (2004) Episodic diamond genesis at Jwaneng, Botswana, and implications for Kaapvaal craton evolution. *Lithos* **77**(1), 143–154.

Richardson S. H., Pöml P. F., Shirey S. B. and Harris J. W. (2009) Age and origin of peridotitic diamonds from Venetia, Limpopo Belt, Kaapvaal-Zimbabwe craton. *Lithos* **112**, 785–792.

Saunders J. E., Pearson N. J., O'Reilly S. Y. and Griffin W. L. (2015) Sulfide metasomatism and the mobility of gold in the lithospheric mantle. *Chem. Geol.* **410**, 149–161.

Schrauder M., Koeberl C. and Navon O. (1996) Trace element analyses of fluid-bearing diamonds from Jwaneng, Botswana. *Geochimica et Cosmochimica Acta* **60**(23), 4711–4724.

Shirey S. B., Carlson R. W., Richardson S. H., Menzies A., Gurney J. J., Pearson D. G., Harris J. W. and Wiechert U. (2001) Archean emplacement of eclogitic components into the lithospheric mantle during formation of the Kaapvaal Craton. *Geophys. Res. Lett.* **28**(13), 2509–2512.

Shirey S. B., Harris J. W., Richardson S. H., Fouch M. J., James D. E., Cartigny P., Deines P. and Viljoen F. (2002) Diamond genesis, seismic structure, and evolution of the Kaapvaal-Zimbabwe craton. *Science* **297**(5587), 1683–1686.

Shirey S. B., Richardson S. H. and Harris J. W. (2004) Integrated models of diamond formation and craton evolution. *Lithos* **77** (1), 923–944.

Shirey S. B., Cartigny P., Frost D. J., Keshav S., Nestola F., Nimis P., Pearson D. G., Sobolev N. V. and Walter M. J. (2013) Diamonds and the geology of mantle carbon. *Rev. Mineral. Geochem.* **75**(1), 355–421.

Silver P. G., Fouch M. J., Gao S. S. and Schmitz M. (2004) Seismic anisotropy, mantle fabric, and the magmatic evolution of Precambrian southern Africa. *S. Afr. J. Geol.* **107**(1–2), 45–58.

Simelane V. G. (2004). *Palmietgat kimberlite pipes, South Africa: clues to the nature and origin of the sub-Bushveld Kaapvaal Craton*. University of the Witwatersrand, MSc thesis.

Smith J. W., Holwell D. A. and McDonald I. (2014) Precious and base metal geochemistry and mineralogy of the Grasvally Norite-Pyroxenite-Anorthosite (GNPA) member, northern Bushveld Complex, South Africa: implications for a multistage emplacement. *Miner. Deposita* **49**, 667–692.

Sobolev N. V. (1977) Deep-seated inclusions in kimberlites and the problem of the composition of the Upper Mantle. *Am. Geophys. Union*, 83–153.

Stachel T. and Harris J. W. (2008) The origin of cratonic diamonds—constraints from mineral inclusions. *Ore Geol. Rev.* **34**(1), 5–32.

Stachel T. and Luth R. W. (2015) Diamond formation—where, when and how? *Lithos* **220**, 200–220.

Taylor L. A. and Anand M. (2004) Diamonds: time capsules from the Siberian Mantle. *Chemie der Erde-Geochemistry* **64**(1), 1–74.

Taylor L. A. and Liu Y. (2009) Sulfide inclusions in diamonds: not monosulfide solid solution. *Russ. Geol. Geophys.* **50**, 1201–1211.

Thomassot E., Cartigny P., Harris J. W. and Viljoen K. F. (2007) Methane-related diamond crystallization in the Earth's mantle: stable isotope evidences from a single diamond-bearing xenolith. *Earth Planet. Sci. Lett.* **257**(3), 362–371.

Thomassot E., Cartigny P., Harris J. W., Lorand J. P., Rollion-Bard C. and Chaussidon M. (2009) Metasomatic diamond growth: a multi-isotope study (^{13}C, ^{15}N, ^{33}S, ^{34}S) of sulphide inclusions and their host diamonds from Jwaneng (Botswana). *Earth Planet. Sci. Lett.* **282**(1), 79–90.

Vlassenbroeck J., Dierick M., Masschaele B., Cnudde V., Van Hoorebeke L. and Jacobs P. (2007) Software tools for quantification of X-ray microtomography at the UGCT. *Nucl. Instr. Methods Phys. Res. A* **580**(1), 442–445.

Wainwright A. N., Luguet A., Schreiber A., Fonseca R. O. C., Nowell G. M., Lorand J.-P., Wirth R. and Janney P. E. (2016) Nanoscale variations in ^{187}Os isotopic composition and HSE systematics in a Bultfontein peridotite. *Earth Planet. Sci. Lett.* **447**, 60–71.

Westerlund K. J., Gurney J. J., Carlson R. W., Shirey S. B., Hauri E. H. and Richardson S. H. (2004) A metasomatic origin for late Archean eclogitic diamonds: implications from internal morphology of diamonds and Re-Os and S isotope characteristics of their sulfide inclusions from the late Jurassic Klipspringer kimberlites. *S. Afr. J. Geol.* **107**(1–2), 119–130.

Westerlund K. J., Shirey S. B., Richardson S. H., Carlson R. W., Gurney J. J. and Harris J. W. (2006) A subduction wedge origin for Paleoarchean peridotitic diamonds and harzburgites from the Panda kimberlite, Slave craton: evidence from Re-Os isotope systematics. *Contrib. Miner. Petrol.* **152**, 275–294.

Wiggers de Vries D. F., Pearson D. G., Bulanova G. P., Smelov A. P., Pavlushin A. D. and Davies G. R. (2013) Re-Os dating of sulphide inclusions zonally distributed in single Yakutian diamonds: evidence for multiple episodes of Proterozoic formation and protracted timescales of diamond growth. *Geochim. Cosmochim. Acta* **120**, 363–394.

Yefimova E. S., Sobolev N. V. and Pospelova L. N. (1983) Vklyucheniya sul'fidov v almazakh i osobennosti ikh paragenezisa. Sulfide inclusions in diamonds and their paragenesis. *Zap Vses Miner Obshch* **112**, 300–310.

Associate editor: Amy J.V. Riches